

Project 010 Aircraft Technology Modeling and Assessment

Georgia Institute of Technology and Purdue University

Project Lead Investigators

Dimitri Mavris (PI)
Regents Professor
School of Aerospace Engineering
Georgia Institute of Technology
Mail Stop 0150
Atlanta, GA 30332-0150
404-894-1557
dimitri.mavris@ae.gatech.edu

William Crossley (PI)
Professor
School of Aeronautics and Astronautics
Purdue University
701 W. Stadium Ave
West Lafayette, IN 47907-2045
765-496-2872
crossley@purdue.edu

Jimmy Tai (Co-PI)
Senior Research Engineer
School of Aerospace Engineering
Georgia Institute of Technology
Mail Stop 0150
Atlanta, GA 30332-0150
404-894-0197
jimmy.tai@ae.gatech.edu

Daniel DeLaurentis (Co-PI)
Professor
School of Aeronautics and Astronautics
Purdue University
701 W. Stadium Ave
West Lafayette, IN 47907-2045
765-494-0694
ddelaure@purdue.edu

University Participants

Georgia Institute of Technology

- PI(s): Dr. Dimitri Mavris (PI), Dr. Jimmy Tai (Co-PI)
- FAA Award Numbers: 13-C-AJFE-GIT-006, 13-C-AJFE-GIT-012, 13-C-AJFE-GIT-022, 13-C-AJFE-GIT-031, 13-C-AJFE-GIT-37, 13-C-AJFE-GIT-041, 13-C-AJFE-GIT-50, 13-C-AJFE-GIT-52, 13-C-AJFE-GIT-56, 13-C-AJFE-GIT-76, 13-C-AJFE-GIT-94
- Period of Performance: September 1, 2021 to August 31, 2022

Purdue University

- PI(s): Dr. William A. Crossley (PI), Dr. Daniel DeLaurentis (Co-PI)
- FAA Award Numbers: 13-C-AJFE-PU-004, 13-C-AJFE-PU-008, 13-C-AJFE-PU-013, 13-C-AJFE-PU-018, 13-C-AJFE-PU-026, 13-C-AJFE-PU-032, 13-C-AJFE-PU-035, 13-C-AJFE-PU-044, 13-C-AJFE-PU-047
- Period of Performance: September 1, 2021 to August 31, 2023

Project Funding Level

The project is funded by the FAA at the following levels: Georgia Institute of Technology: \$700,000; Purdue University is continuing on a no-cost extension. Cost-sharing details are below:

The Georgia Institute of Technology has agreed to a total of \$700,000 in matching funds. This total includes in-kind cost-sharing from Boom Supersonics; salaries for the project director, research engineers, and graduate research assistants (GRAs); and funding for computing, financial, and administrative support, including meeting arrangements. The institute has also agreed to provide tuition remission for the students, paid by state funds.

The most recent FAA funding to Purdue University for this project was a total of \$225,000. Purdue provides matching support through salary support for the faculty PIs, and through salary support and tuition and fee waivers for one of the GRAs working on this project. OAG Aviation Worldwide Limited also provided in-kind cost-sharing to the Purdue team. The total of this matching is \$225,000.

Investigation Team

Georgia Institute of Technology

- PI: Dimitri Mavris
- Co-investigator: Jimmy Tai
- Vehicle modeling technical leads (Research Faculty): Jai Ahuja, Christian Perron, Chung Lee, Brennan Stewart
- Fleet modeling technical lead (Research Faculty): Holger Pfaender
- AEDT modeling technical leads (Research Faculty): Dushhyanth Rajaram, Michelle Kirby, Ameya Behere
- Graduate students: Nikhil Iyengar, Barbara Sampaio, Edan Baltman, Joao De Azevedo, Jiajie (Terry) Wen, Ted Vlady, Zayne Roohi and Srikanth Tindivanam Varadharajan

Purdue University

- PI: William Crossley
- Co-investigator: Daniel DeLaurentis
- Research faculty: Muharrem Mane
- Graduate students: Samarth Jain, Suzanne Swaine, Tien-Yueh Fung, Boning Yang, and Katelin Zichittella

Project Overview

Georgia Institute of Technology (Georgia Tech) and Purdue University have partnered to investigate the future demand for supersonic air travel and the environmental impact of supersonic transports (SSTs). In the context of this research, environmental impacts include direct carbon dioxide (CO₂) emissions, noise, and fuel consumption. The research is conducted as a collaborative effort to leverage the capabilities and knowledge available from the multiple entities that make up the ASCENT university partners and advisory committee. The primary objective of this research project is to support the FAA in modeling and assessing the potential future evolution of the next-generation supersonic aircraft fleet. The research in this project consists of five integrated focus areas: (a) establishing fleet assumptions and performing demand assessment (completed last year); (b) performing preliminary SST environmental impact prediction (ongoing); (c) developing modeling approaches to model SSTs within the FAA Aviation Environmental Design Tool (AEDT); (d) performing vehicle and fleet assessments of potential future supersonic aircraft; and (e) performing physics based modeling of SSTs and performing conceptual design using the Framework for Advanced Supersonic Transport (FASST).

To better understand the potential demand for supersonic air travel, the team developed a parametric airline operating-cost model to explore the sensitivities of key vehicle, operational, and cost parameters on the required yield that an airline would need to target for ticket prices on potential new supersonic aircraft. The current model, however, assumes fixed parameters for key vehicle metrics, which can be changed but do not include sensitivities to key vehicle design choices such as vehicle

size, design cruise Mach number, and maximum range. This task will examine the implications of the physical and technical dependencies on airline operational cost. Through the vehicle performance sensitivities, such as passenger capacity and design cruise Mach number, the combined “sweet spot,” i.e., the most profitable vehicle for an airline to operate, can be determined. To accomplish this goal, the existing vehicle models created in the prior year will be utilized and supplemented with the additional vehicles proposed in this period of performance. These vehicles together will serve as the foundation to create credible sensitivities regarding parameters such as vehicle size and design cruise Mach number. These sensitivities will then be embedded in the airline operating-cost estimation model and used to explore the combined vehicle and airline operational space to identify the most economically feasible type of supersonic vehicle.

In an independent complementary approach, to consider the demand and routes for supersonic aircraft, the Purdue team developed a ticket pricing model for possible future supersonic aircraft that relies on the “as-offered” fares, before the novel coronavirus (COVID-19) pandemic, for business-class and first-class tickets on routes expected to have passenger demand for supersonic aircraft. Via an approach considering the number of passengers potentially demanding fares at business class or above on a city-pair route, the distance of that city-pair route, an adjustment to increase the over-water distance of the route where the aircraft can fly supersonically to allow for the shortest trip time, and the range capability of a low-fidelity modeled medium SST (55-passenger capacity) to fly that route with the shortest trip time, the Purdue team identified a network among 257 airports that could potentially allow for supersonic aircraft service in a network of routes with at least one end (i.e., the origin or destination) in the United States (US).

Work undertaken this year included expanding the US-touching network to a worldwide network. This change to a worldwide network required the identification of a global fleet of aircraft (type and number of aircraft) as well as the passenger demand on each route. By providing these potential routes as input to the Fleet-Level Environmental Evaluation Tool (FLEET) simulation, the allocation problem in FLEET then determines which routes would be profitable for the airline to offer supersonic transportation and how many supersonic aircraft would operate on these routes, providing a prediction of which routes might have supersonic aircraft use and the number of supersonic flights operated on those routes at dates in the future. Because of the evolution of the existing fleet of subsonic aircraft and changes to the cost-estimation module of NASA’s FLight Optimization System (FLOPS), the Purdue team developed an acquisition and operating cost model that is used to estimate these costs for all aircraft modeled in FLEET. During this year’s efforts, the Purdue team also began work to adapt FLEET to analyze the operations and environmental emissions of business jet operations. This task entails estimating travel demand of business jet aircraft, the fleet size and mix that serve that demand, the worldwide network of operations, and the development of the resource allocation model that estimates the optimal utilization of aircraft to satisfy travel demand.

One major accomplishment of the project during the performance period is the preliminary results for the design of a 65-passenger SST cruising at Mach 1.7 for 4,250 nmi. The preliminary results are arrived at through computational fluid dynamics (CFD)-based vehicle shape optimization, engine cycle modeling using Numerical Propulsion System Simulation (NPSS), and noise modeling using NASA’s Aircraft Noise Prediction Program (ANOPP), and mission analysis and detailed takeoff and landing analysis that incorporates variable noise reduction system (VNRS) using FLOPS. These modeling approaches and programs are all integrated into FASST, which allowed Georgia Tech to generate interdependency results between fuel burn (or maximum takeoff weight [MTOW]) and certification cumulative noise levels (in EPNdB; effective perceived noise in decibels). The other major accomplishment is Georgia Tech’s support of the environmental assessment (EA) study of Greensboro airport in order for a potential supersonic airframe manufacturer to perform flight tests. The EA study required Georgia Tech to model a generic transport SST that is representative of the potential supersonic airframer’s concept except with marginal noise characteristics (small cumulative noise margin). The rationale is to account for noise at the current limiting, highest-noise case (bounded within the existing subsonic, Stage 5 noise certification limits of compliance) so that developmental SST configurations operated at or below this upper MTOW can be built, tested, and refined to these noise goals. Georgia Tech generated all the necessary performance attributes and imported them into AEDT to generate noise contours for Greensboro. Both the vehicle performance and AEDT databases are provided to the FAA, who in turn worked with Greensboro airport to perform the actual environmental assessment. The final major accomplishment during the period of performance is the development of a methodology to construct regression models to be used in the full-flight simulation for FAA’s AEDT. The current method is to rely on a base of aircraft data (BADA) databases; however, there is currently no BADA database for supersonic transports. Georgia Tech has successfully developed a regression methodology to predict fuel burn, net thrust, and drag coefficient values over the entire span of mission.

Purdue used its FLEET tool to produce initial estimates of the fleet-level impact of future supersonic aircraft operating on the worldwide network. The SSTs required for these fleet-level analyses were provided by the Georgia Tech vehicle modeling tasks with FASST, to maintain consistent aircraft modeling throughout the project. The studies provide a glimpse into future

supersonic air travel by using physics-based models of supersonic vehicle performance. Future work should build on current estimates to conduct more detailed vehicle and fleet performance.

Project Introduction

Georgia Tech and Purdue partnered to investigate the effects of supersonic aircraft on the future environmental impacts of aviation. Impacts assessed at the fleet level include direct CO₂ emissions and fuel consumption. The research is conducted as a collaborative effort to leverage capabilities and knowledge available from the multiple entities that make up the ASCENT university partners and advisory committee. The primary objective of this research project is to support the FAA in modeling and assessing the potential future evolution of the next-generation supersonic aircraft fleet.

Milestones

Georgia Tech had three milestones for this year of performance:

1. Generate interdependency results showing trades between fuel burn and cumulative noise levels
2. Support FAA in an EA using FASST and AEDT
3. Provide FASST SST descriptions and characteristics in Microsoft PowerPoint format

For Purdue, the proposal covering this year of performance included several milestones:

1. Update the aircraft cost coefficients
2. Expand the FLEET route network to include global routes
3. Analysis of alternate SST aircraft concepts
4. Develop a FLEET-like model to analyze business jet operations

Previously, the aircraft cost information needed for FLEET simulations, including the acquisition and operating costs, were generated using the cost module in FLOPSv8. The cost module is no longer available in FLOPSv9, which both Purdue and Georgia Tech are using for vehicle sizing and performance estimation, so a new cost model with similar functionality was needed and developed during this year's effort.

To increase the utility of FLEET and the insights that can be gained by analyzing the introduction of an SST into the fleet, the Purdue team expanded the network of operations from the US-touching network to a global network. The airports in the network are still the original 257 airports, but the routes among them in the FLEET network now include all global routes with regularly scheduled service. This update to FLEET also included the identification of the worldwide size and mix of aircraft used by airlines to provide service and meet passenger demand.

Finally, the team began work to enable the analysis of environmental emissions and impact of a supersonic business jet on operations. This entails the creation of a FLEET-like tool that mirrors the analysis of airline operations but is adapted to capture the features of business jet operations.

Major Accomplishments

Major accomplishments of the project during the period of performance include the generation of preliminary results for the design of a 65-passenger SST cruising at Mach 1.7 for 4,250 nmi, with interdependency results between fuel burn (or maximum takeoff weight) and certification cumulative noise levels (in EPNdB). These results were obtained through CFD based aerodynamic shape optimization of the aircraft geometry, NPSS engine modeling, noise modeling in ANOPP, and mission analysis coupled with detailed takeoff and landing analysis incorporating VNRS through FLOPS.

In addition, Georgia Tech supported the EA study of the Greensboro airport in order for a potential supersonic airframe manufacturer to perform flight tests. This was accomplished by modeling a generic SST representative of the potential supersonic airframer's concept except with a small cumulative noise margin Georgia Tech generated all the necessary performance attributes and imported them into AEDT to generate noise contours for Greensboro, shared these databases with the FAA, who in turn worked with Greensboro airport to perform the actual environmental assessment. Lastly, Georgia Tech developed a methodology to construct regression models to be used in the full-flight simulation for FAA's AEDT, sidestepping the current way of relying on BADA databases, which do not even exist for supersonic transports. As such, this methodology can now predict fuel burn, net thrust, and drag coefficient values over an entire mission flight envelope.

One major accomplishment of the Purdue team during this year's effort was the successful expansion of the network of operations from 1,149 US-touching routes among 257 airports to 5,503 worldwide routes; this increases the analytical capability of FLEET and enables a more comprehensive assessment of the impact of supersonic transportation on the environment. The updated FLEET models can identify routes on which an SST can provide profit to airline operations and the associated environmental emissions. Because of the available data, this update also moved the FLEET baseline year of analysis from 2005 to 2011. With the addition of more historical data, which includes the impact of COVID-19 on airline operations and travel demand in 2020 and 2021, the demand and emissions projections until 2050 are more realistic.

Task 1 - SST Aerodynamic Modeling

Georgia Institute of Technology

Objectives

There are two primary objectives of the SST aerodynamic modeling task:

- Aerodynamic shape optimization of the SST outer mold line (OML) for a given cruise Mach number (for a fixed planform area and wing capture area)
- Generation of parametric drag polars for the optimized vehicle that capture aerodynamic performance across the entire flight envelope as a function of wing planform area and inlet capture area

Research Approach

Analysis Workflow

A general analysis process was developed to obtain the aerodynamic performance of multiple aircraft designs. This process was then automated with Python and implemented by using Georgia Tech's high-performance computing facilities. Because the analysis workflow was automated and easily parallelizable, many designs could be analyzed at once. Hundreds of aerodynamic analyses could be completed in a matter of hours, allowing for rapid evaluation of designs and generation of drag polars.

Starting from a set of design variables, the first step was to generate a computer-aided design (CAD) representation of the aircraft geometry. This process was done using Engineering Sketch Pad (ESP), a lightweight, open-source CAD tool developed by MIT [1]. ESP allows users to easily script generation of complex geometries and to expose design parameters. Therefore, changing global parameters, such as the sweep angle or taper ratio, would automatically and seamlessly scale and reposition the different sections of the wing. After a new geometry was defined, it was then saved to a generic CAD file (the EGADS format in the current workflow) and tessellated for later use in CFD analysis.

The OML is tailored to maximize lift/drag (L/D) at the design cruise Mach number as a surrogate to minimize mission fuel burn. The optimization is broken down into three stages: two initial phases focusing on the fuselage and vertical tail (VT) design, and one main stage focusing on the wing planform optimization. Both inviscid (Euler) and Reynolds-Averaged Navier-Stokes (RANS) CFD analyses are used in a multi-fidelity optimization approach to reduce design time and cost. NASA's Cart3D [2] is the inviscid solver used and Siemens' STAR-CCM+ [3] is the RANS solver used. The following sections detail each airframe design phase.

Fuselage Design

Using the number of passengers set by requirements, the fuselage design, in terms of minimum cabin length and width requirements, is constrained by the cabin layout. While slender fuselages are preferable for supersonic cruise performance, care must be taken to avoid an excessively long body, as takeoff rotation constraints necessitate longer and thus heavier landing gears. Once the cabin layout is frozen, additional refinements are conducted on the fuselage nose and tail cone sections, in terms of length and cross-sectional radius, to optimize for cruise L/D. During this fuselage design process, the wing planform is frozen. A design of experiments (DoE) is developed, with the length of the nose, length of the tail, and cross-sectional radii for various stations of the fuselage as independent variables. CART3D with a single-pass viscous correction is used for the aerodynamic analysis. The results from this DoE are used to train a neural network surrogate, which in turn is used to optimize the vehicle for cruise L/D. The resulting fuselage design is then frozen and used in the wing optimization stage.

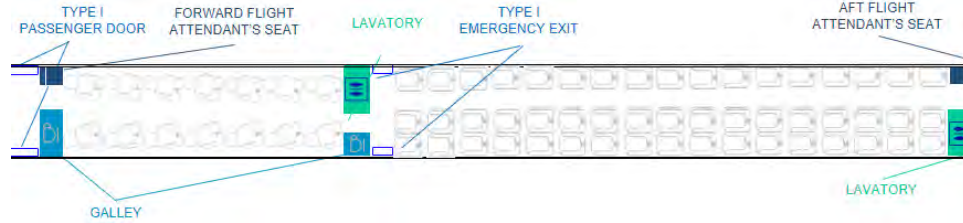


Figure 1. Cabin layout for a 65-passenger aircraft.

Vertical Tail Design

The VT is designed primarily based on two critical Federal Aviation Regulations (FAR): §25.147 for directional control under two-engine inoperative (2EI) conditions and §25.237 for crosswind requirements. Directional stability is analyzed using first-order principles and semi-empirical relations, rather than CFD. Design variables considered are wing planform area, aspect ratio, taper ratio, leading edge sweep, and thickness to chord. The goal is to find the smallest VT planform area that satisfied the requirements for the furthest feasible VT location relative to the wing. A symmetric biconvex airfoil is used, with a thickness-to-chord ratio (t/c) fixed to a value that ensures an adequate cross-sectional thickness for the rudder actuators but is small enough to not penalize supersonic cruise performance. The rudder chord length to mean aerodynamic chord fraction is set to 0.35.

Wing Planform Design

Since the aerodynamic performance of the vehicle is strongly dependent on the wing planform, most of the optimization effort is focused on this component. As such, RANS CFD is used to analyze the performance of each design perturbation. The wing is defined by two sections, inboard and outboard, and five airfoil profiles. Global variables like taper ratio, aspect ratio, sweep, and dihedral apply to the entire wing, whereas the delta variables control the difference between the inboard and outboard sections. The wing break location variable determines the spanwise extent of the inboard section relative to the outboard, for a fixed total span. Biconvex airfoils are used to define the wing, with twist and camber being part of the design space. The maximum camber is limited to half the specified t/c ratio.

Given the dimensionality of the problem and the cost of each function call, there is a need to be strategic about how this optimization exercise is carried out. As such, a gradient-free active subspace approach is first used to reduce the dimensionality of the design space using less expensive inviscid CFD. Then, adaptive sampling is performed in this reduced design space with RANS simulations to improve the L/D . A high-level overview of this process is shown in Figure 2. The goal of the active subspace method [4] is to reduce the high-dimensional input space of some function to a lower-dimensional subspace, the so-called active subspace. For instance, given a function $f(\mathbf{x})$, where $\mathbf{x} \in \mathbb{R}^d$ is a high-dimensional input vector, the following approximation is made:

$$f(\mathbf{x}) \approx g(\mathbf{z}) = g(\mathbf{W}^T \mathbf{x}) \quad (1)$$

where $g(\mathbf{z})$ is an approximate predictor of $f(\mathbf{x})$, and $\mathbf{W} \in \mathbb{R}^{d \times k}$ is a projection matrix that maps the inputs \mathbf{x} to a low-dimensional representation $\mathbf{z} \in \mathbb{R}^k$, which are referred to as the active variables with $k < d$. In other words, the active subspace method aggregates potentially many design variables into a few modes that best capture the variability of the output. As a result, optimization with respect to the active variables is more efficient because the size of the design space is exponentially reduced. Fitting a surrogate to predict the output of interest is also made easier as the active subspace alleviates the infamous “curse of dimensionality.” The main difficulty of the active subspace method is in finding the matrix \mathbf{W} that best approximates the variability of $f(\mathbf{x})$. Although most dimensionality reduction methods are unsupervised, the active subspace is a supervised approach. This implies that the reduction of the input spaces is not based on the similarity between design vectors; rather, it is informed by the functional dependence between the input and the output spaces.

The classical active subspace approach for dimensionality reduction proposed by Constantine relies on gradient information of the objective function, which can be challenging to obtain. Gradient-free approaches have been proposed in the literature [5, 6, 7], but these methods require extensive sampling of the objective function, which can be costly in scenarios where the objective is being evaluated by high-fidelity codes like RANS solvers. To counter this drawback, Mufti et al. [8] have proposed a gradient-free and multi-fidelity approach whereby a lower fidelity and relatively cheaper code, in this case Cart3D, is used to extract an approximation of the RANS active subspace. The requirement for this approach is an initial DoE that samples the design space. Each case in this DoE is evaluated in Cart3D and L/D is recorded. The proposed multi-fidelity

approach is then applied to obtain a reduced representation of the design variables based on the lower fidelity results. Although the inviscid L/D results from Cart3D are not as accurate as those obtained with RANS, both tend to have similar behaviors. Therefore, it is reasonable to assume that an active subspace computed using inviscid results is a good representation of the corresponding subspace that would be obtained with RANS results. Mufti et al. have demonstrated that this assumption holds for the design of transonic airfoils and wings. Although using lower fidelity results to compute the active subspace has drawbacks and does reduce the accuracy of the method, it also significantly reduces the cost of computing the active subspace. For the purposes of this work, this tradeoff between accuracy and computational cost is considered acceptable.

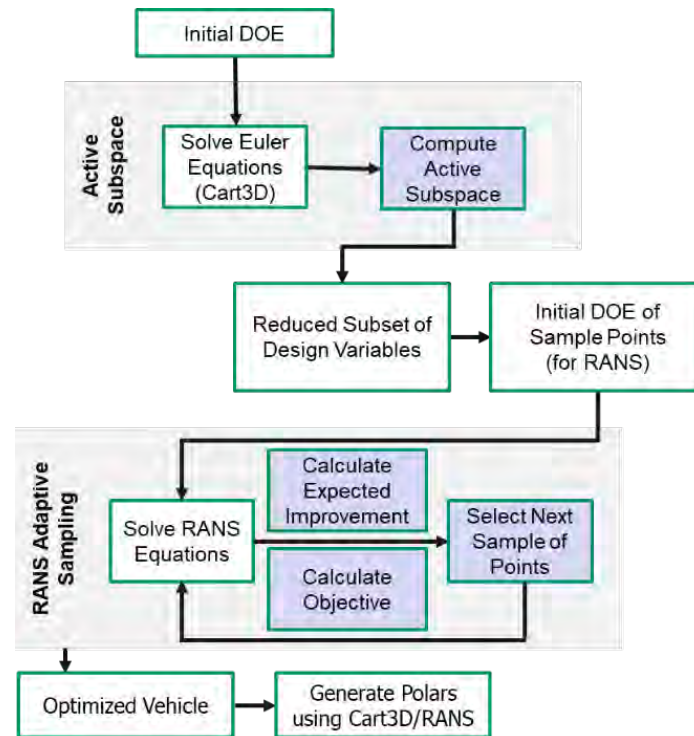


Figure 2. Aerodynamic optimization process. DOE, design of experiments; RANS, Reynolds-Averaged Navier-Stokes.

Once the reduced representation of the design variables is determined, the RANS optimization process begins. The objective function is maximized through an adaptive sampling approach, using the efficient global optimization (EGO) method [9]. To start the process, a warm-start DoE is run to train a Kriging surrogate model. The Kriging model not only provides a prediction of the objective function at nonsampled points, but it also provides an estimate for the model prediction uncertainty between two sampled points. These two ingredients are used in the EGO method to balance “exploration” vs “exploitation” of the design space. In the current context, “exploration” refers to sampling in regions where model uncertainty is high, and “exploitation” denotes sampling in regions close to the optimum. After the initial warm-start DoE and model training, a small number of candidate points are selected that maximize the “expected improvement” criterion of the objective function. These samples are then evaluated in RANS, the Kriging model is retrained, the expected improvement is recomputed, and the process repeats until a user-defined stopping condition is met. In this fashion, the aerodynamic performance of the vehicle is improved iteratively. The sample size of the warm-start DoE and the number of additional samples required is dependent on the dimension of the design space and, as such, the active subspace dimensionality reduction in the previous step is critical for minimizing the overall design time and cost.

Note that for some vehicles, the optimization process would converge on a wing design with an excessive sweep and aspect ratio. The resulting vehicle would then have a large wing weight during the system analysis, which would severely hinder mission performance. This is because the wing planform design is purely aerodynamic and lacks any structural consideration. To circumvent this issue, an upper limit on wing weight has been added to the adaptive sampling approach. As a result, the

EGO algorithm searches for new samples that maximize the expected improvement of the objective while having a high probability of meeting the wing weight constraint following the process described in [10]. For this purpose, the wing weight is estimated from a given planform using the FLOPS weight equations [11]. From these weight estimates, an additional Kriging model is trained, which is then used to predict the likelihood of a new design to satisfy the weight constraint. Figure 3 shows an example of a design optimized without and without the wing weight constraint.

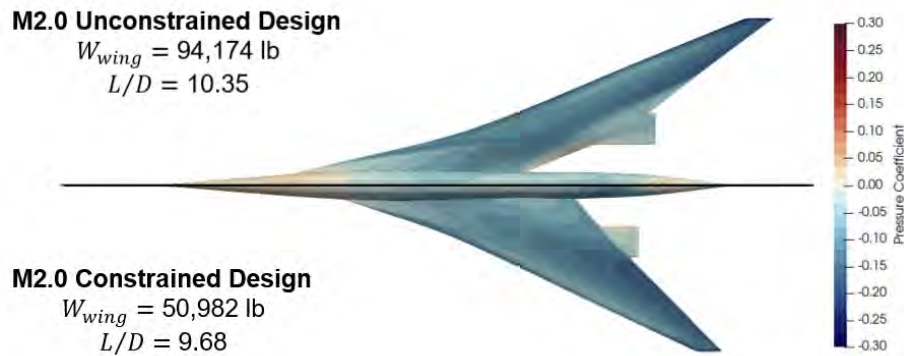


Figure 3. Comparison between an unconstrained and a wing weight-constrained optimum. W_{wing} , wing weight; L/D , lift-to-drag ratio.

Drag Polar Generation for Optimized Vehicle

Once the vehicle with the highest cruise L/D is obtained, to enable mission analysis, drag polars for every point in the operating envelope are generated in the form of a table with Mach, altitude, lift coefficient (C_L), and drag coefficient (C_D) as the columns. Generating a drag polar that covers the entire envelope is quite costly to perform solely with RANS CFD. Therefore, a hybrid approach is used, as shown in Figure 4. First, the less expensive Cart3D is used to generate a set of “baseline polars” for all Mach number and angle-of-attack (AoA) combinations. Note that since Cart3D is an inviscid solver, altitude is not an input because it only impacts viscous forces. RANS CFD is then used to sample a subset of the low-fidelity flight conditions. In this case, a total of 15 RANS samples are considered. The flight conditions for these RANS cases were chosen strategically to minimize the root mean square error of the surrogate model and the number of high-fidelity cases required to achieve that. Because altitude was not a consideration for the low-fidelity CFD, random values were assigned to each RANS sample in a way that spread them out uniformly in the expected range of Reynolds number. These viscous results are then used to calibrate the inviscid polars to account for viscous effects. This is achieved using hierarchical Kriging [12], which is a type of multi-fidelity surrogate model. In this situation, the low-fidelity data are the numerous Cart3D results and the high-fidelity samples are the few RANS CFD solutions.

Parametric Drag Polars Capturing Impacts of Changing Wing Planform Area and Inlet Capture Area

Aerodynamic optimization is conducted for a fixed-wing planform area and inlet capture area. However, as part of vehicle sizing and mission analysis, both the engine size and wing planform area are allowed to scale. To account for the impacts of these changes on the aerodynamic performance of the vehicle, it is desirable to have a set of drag polars that are a function of these design variables. This objective is efficiently achieved through a proper orthogonal decomposition (POD) reduced-order model (ROM).

A parametric ROM approximates the prediction of a function by mapping an m -dimensional input vector to a d -dimensional output vector. Unlike a conventional surrogate model, the quantity being predicted is a high-dimensional vector. The development of parametric drag polars at a high level is illustrated in Figure 5 and mostly follows the work shown in [13], where a similar approach was used for a parametric engine deck. The main steps are as follows: First, a DoE is created to sample the design space spanned by wing planform area and inlet capture area. A total of 10 samples are defined with unique combinations of the two design variables. The nacelle length is correlated with the inlet capture area and is thus a fallout. A multi-fidelity mission drag polar is generated for each of the samples in the DoE using the process outlined in the preceding section. These drag polars are then used as observations to train the ROM. Once the modes and coefficients for the POD model are obtained, a radial basis function is used as the interpolating mechanism for the POD coefficients such that drag polars can be predicted at previously unseen values of the design variables.

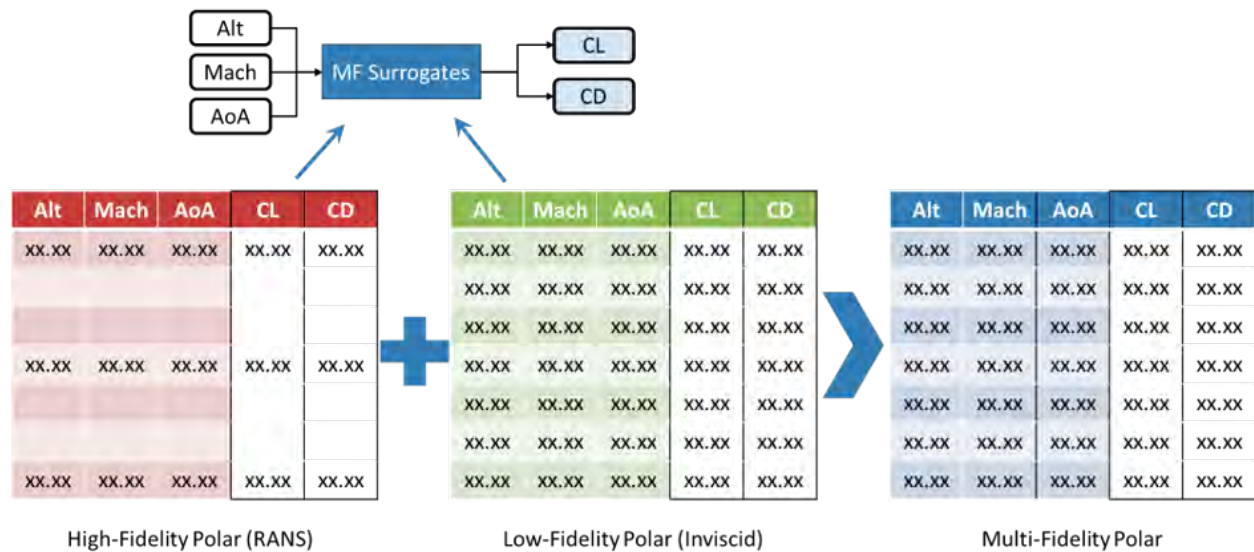


Figure 4. Schematic depicting multi-fidelity drag polar generation process. Alt, altitude; AoA, angle of attack; MF, multi-fidelity; CL, lift coefficient; CD, drag coefficient.

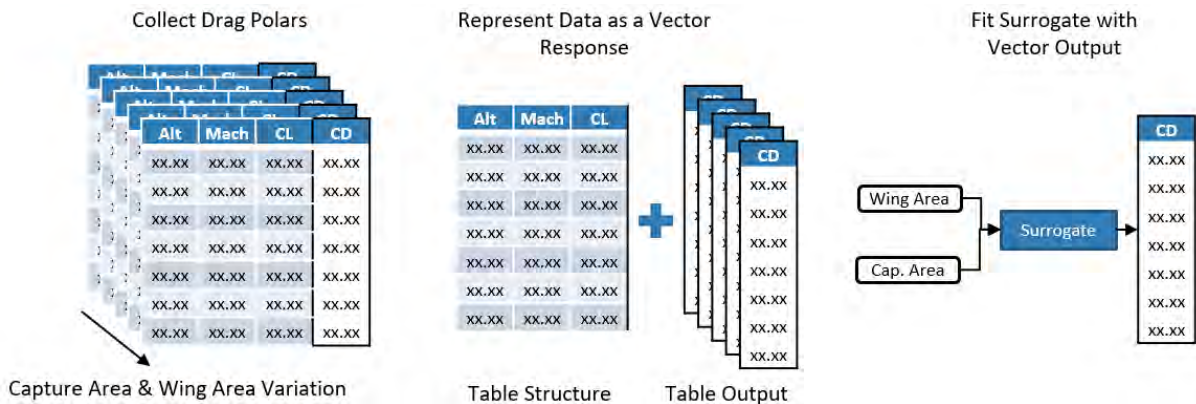


Figure 5. Schematic demonstrating the construction of the parametric drag polars. Alt, altitude; CL, lift coefficient; CD, drag coefficient.

Results

Fuselage Design

Table 1 shows the variables and ranges for the fuselage OML DoE. Figure 6 shows the L/D trends against each of the design variables at the design point that maximizes cruise L/D. Analysis of the DoE results through the surrogate model reveals a plateau in L/D for the nose length variable and a natural maximum for the tail length. The radius at the start of the cabin, the radius at two-thirds cabin length, and the radius at the end of the cabin have a peak cruise L/D at the minimum allowed value due to the cabin constraint. The radius at one-third cabin length does not have a peak cruise L/D at the minimum radius, and instead has a maximum cruise L/D at 1.2 times the minimal allowed radius. The radius at the midpoint of the tail does have a peak L/D at the upper bound of the design range.

Table 1. Fuselage outer mold line design of experiments.

Parameter	Min Value	Max Value	Parameter	Min Value	Max Value
Nose length	200 in	1,200 in	Radius at 1/3 of cabin length	54 in	81 in
Cabin length	1,122 in	1,122 in	Radius at 2/3 of cabin length	54 in	81 in
Tail length	200 in	1,200 in	Radius at end of cabin	54 in	81 in
Radius at start of cabin	54 in	81 in	Radius at midpoint of tail	12.5 in	37.5 in

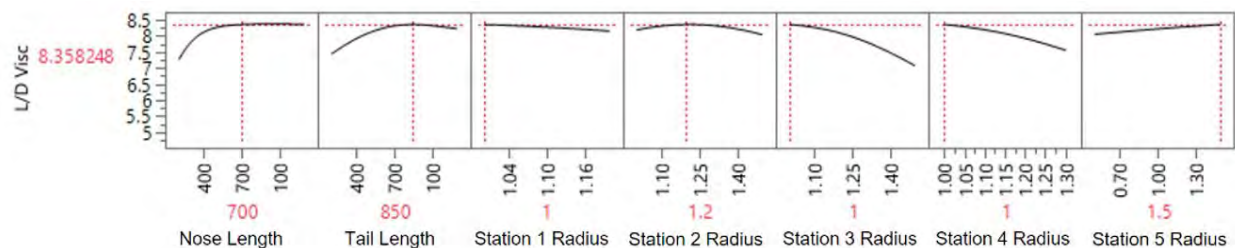


Figure 6. Profiler of fuselage design of experiment surrogate model.

Vertical Tail Design

The chosen VT planform area is 375 ft², which requires a 28° rudder deflection under two-engine inoperative (2EI) conditions defined by FAR §25.147. This deflection is 2° lower than the assumed reasonable limit of 30° and thus provides a buffer. Figure 7 shows the rudder deflection required as a function of VT planform area to maintain a straight heading under 2EI conditions (left), along with the rudder deflection required as a function of crosswind speed (right). The sub-figure on the right in Figure 7 shows that to satisfy FAR §25.237, a rudder deflection of approximately 15° at 25 kts crosswinds is needed, which is well below the assumed limit of 30°. Table 2 presents a summary of the final VT design parameters.

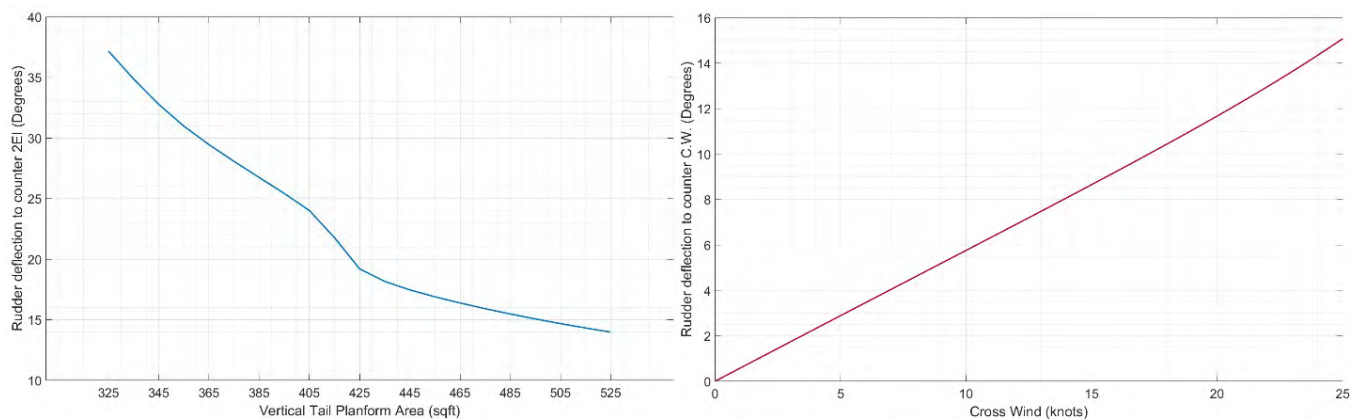


Figure 7. Rudder deflection required to counter yaw from two-engine inoperative (2EI; left) and crosswind (C.W.; right) conditions.

Table 2. Vertical tail design parameters.

Vertical Tail Parameter	Value
Planform area (ft ²)	375
Aspect ratio	1.5
Taper ratio	0.25
Leading edge sweep (degrees)	45
Thickness to chord (average)	0.04

Mach 1.7 Vehicle Wing Design

For this study, the planform area of the wing is fixed at 5,125 ft². In total, there are 18 geometric variables (Table 3) with angle of attack being the 19th design variable. One hundred warm-start cases are executed to sample the design space initially, followed by an additional 100 adaptive samples. The adaptive sampling is stopped when the expected improvement in L/D is on the order of 0.01. Figure 8 shows the distribution of L/D over the warm-start and adaptive samples. As depicted in this figure, the majority of the adaptive sampling cases (blue and purple) have L/D values between 9 and 10 at cruise. Some adaptive samples with lower L/D (between 5 and 9) correspond to early points in the adaptive sampling; i.e., during the “exploration phase” of the optimization.

Table 3. Wing design variables and bounds.

Parameter	Lower Bound	Upper Bound	Parameter	Lower Bound	Upper Bound
Overall taper	0.1	0.3	Delta c/4 sweep break [deg]	-20	0
Overall AR	2.25	4	Section 1 (twist, max camber)	[0, 0%]	[1.5, 0.5(t/c)]
Overall c/4 sweep [deg]	40	60	Section 2 (twist, max camber)	[-5, 0%]	[5, 0.5(t/c)]
Overall dihedral [deg]	-5	5	Section 3 (twist, max camber)	[-5, 0%]	[5, 0.5(t/c)]
Delta taper break	0	0.3	Section 4 (twist, max camber)	[-5, 0%]	[5, 0.5(t/c)]
Delta dihedral break [deg]	-5	5	Section 5 (twist, max camber)	[-5, 0%]	[5, 0.5(t/c)]
Wing break location	0.3	0.6			

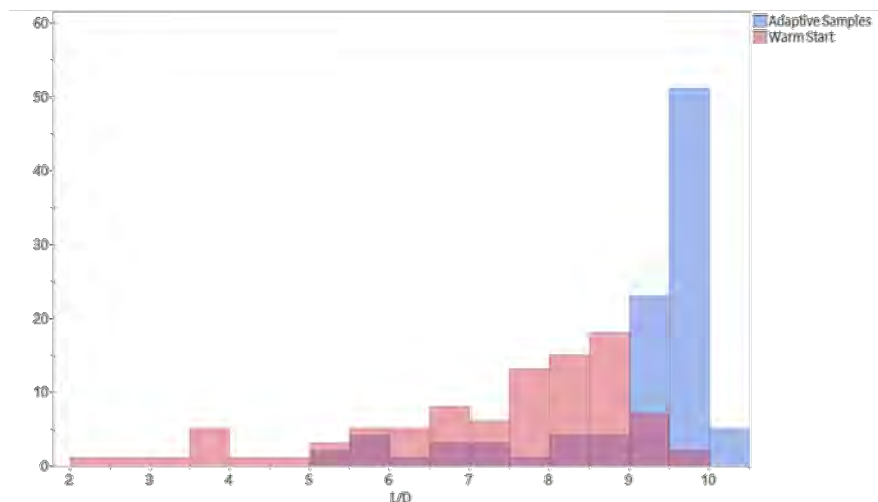


Figure 8. Distribution of lift to drag (L/D) over warm-start and adaptive sampling.

Figure 9 shows a comparison of baseline and optimized wing planforms with the design variable values compared in Table 4. The major differences in the optimized vehicle relative to the baseline are the larger sweep, an inboard shift in the wing

break location, and a change in the twist distribution and camber of the wing. The highest L/D for this vehicle at cruise is 10.16 for a C_L of 0.156, which is a 9.25% improvement over the baseline vehicle peak L/D, which occurs at a C_L of 0.146.

Table 4. Comparison of baseline and optimized wing design variables.

Parameter	Baseline	Optimized	Parameter	Baseline	Optimized
Overall taper	0.1	0.109	Delta dihedral break [deg]	0	0.08
Overall AR	2.5	2.519	Section 1 (twist, max camber)	[0, 0%]	[0.77, 0.92%]
Overall c/4 sweep [deg]	52.5	61.65	Section 2 (twist, max camber)	[0, 0%]	[0.93, 0.34%]
Overall dihedral [deg]	0	-0.62	Section 3 (twist, max camber)	[0, 0%]	[1.44, 0.53%]
Delta taper break	0.2	0.138	Section 4 (twist, max camber)	[0, 0%]	[-2.23, 0.56%]
Delta c/4 sweep break [deg]	-10	-11.60	Section 5 (twist, max camber)	[0, 0%]	[-0.76, 0.42%]
Wing break location	0.45	0.347			

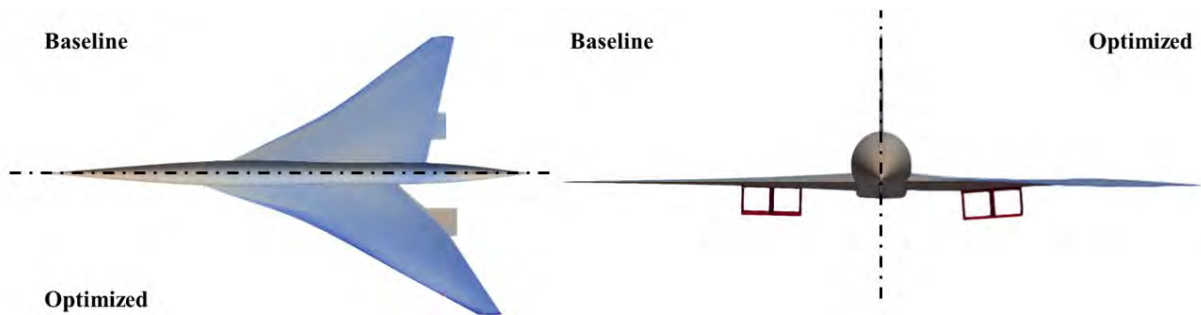


Figure 9. Comparison of baseline and optimized wing planforms.

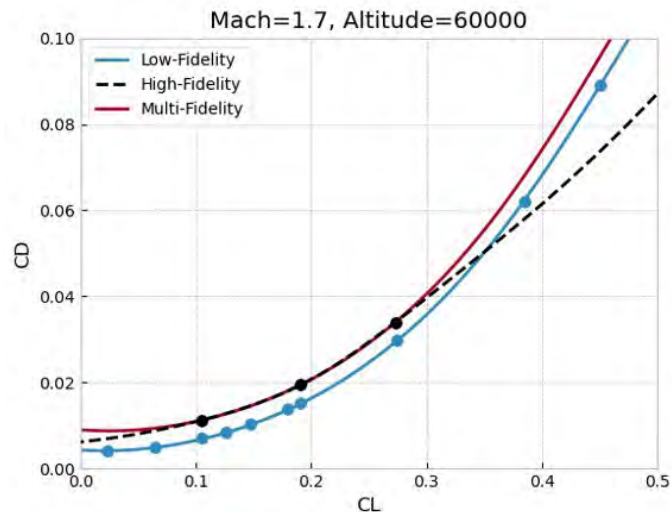


Figure 10. Multi-fidelity drag polar at cruise conditions. CL, lift coefficient; CD, drag coefficient.

Figure 10 shows the multi-fidelity drag polar at cruise conditions for the optimized vehicle. Black points represent the three RANS samples at this flight condition. The high-fidelity curve in this figure shows the drag polar that would have resulted if only the RANS data points were used to fit the surrogate and to extrapolate to the entire flight envelope. Likewise, the blue points are the inviscid data from Cart3D, and the blue low-fidelity curve represents the drag polar obtained from the low-

fidelity data only. The red multi-fidelity curve thus depicts the final drag polar for this vehicle, generated by the multi-fidelity surrogate using both inviscid and RANS data. The effect of the multi-fidelity surrogate can be summarized by an upward shift of the inviscid drag polar, which can be attributed to the effect of friction drag.

Mach 2.0 Vehicle Wing Design

The design of the Mach 2.0 vehicle closely follows the approach described previously for the Mach 1.7 vehicle. The same variable listed in Table 34 was used, 100 warm-start cases were initially generated, and roughly 100 additional cases were adaptively generated until the expected improvement was below a given threshold. However, to accommodate the higher cruise Mach number, the wing sweep bounds were shifted by 10°; i.e., the lower and upper bounds were 50° and 70°, respectively. Also, the optimization of the Mach 2.0 was performed with a constraint on the estimated wing weight. This is because an unconstrained optimization would produce a wing planform with an unreasonably high wing weight. A wing weight upper limit of 53,000 lbs was assumed based on the estimated wing weight of the Mach 1.7 vehicle.

The table below lists the optimized design parameters of the Mach 2.0 aircraft with a wing weight constraint. Many of the parameter values are similar to those of the Mach 1.7 design, with the sweep being noticeably larger, as expected for the higher cruise Mach number. The highest L/D at cruise, among the feasible designs, was 9.68 at a C_L of 0.156. This aerodynamic performance is 4.72% smaller than the Mach 1.7 optimum, which is explained by the higher design cruise speed. Note that this is still higher than the maximum L/D of the baseline. Figure 11 provides a comparison of the Mach 1.7 and 2.0 optima.

Parameter	Baseline	Optimized	Parameter	Baseline	Optimized
Overall taper	0.1	0.098	Delta dihedral break [deg]	0	0.24
Overall AR	2.5	2.607	Section 1 (twist, max camber)	[0, 0%]	[0.86, 0.98%]
Overall c/4 sweep [deg]	52.5	63.63	Section 2 (twist, max camber)	[0, 0%]	[1.30, 0.62%]
Overall dihedral [deg]	0	-0.914	Section 3 (twist, max camber)	[0, 0%]	[0.19, 1.05%]
Delta taper break	0.2	0.199	Section 4 (twist, max camber)	[0, 0%]	[-1.84, 0.86%]
Delta c/4 sweep break [deg]	-10	-7.838	Section 5 (twist, max camber)	[0, 0%]	[-0.74, 0.41%]
Wing break location	0.45	0.347			

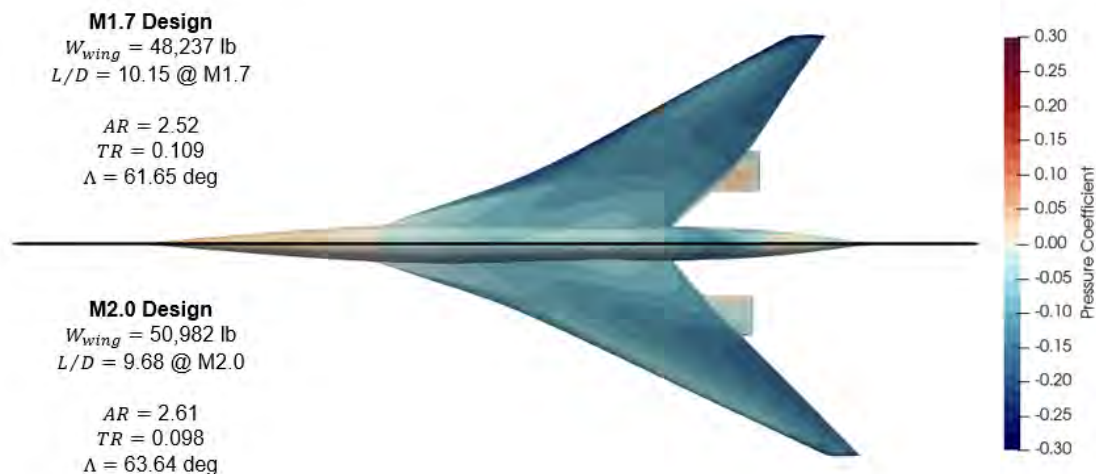


Figure 11. Comparison of the Mach 1.7 and 2.0 optima. W_{wing} , wing weight; L/D, lift-to-drag ratio; AR, aspect ratio; TR, taper ratio; Λ , wing quarter chord sweep.

Task2 - SST Propulsion System Modeling

Georgia Institute of Technology

Objectives

The propulsion system plays an important role on performance metrics, such as fuel burn, gross weight, and takeoff field length, and in environmental metrics, such as noise and emissions. As such, the objective of the propulsion system modeling was to develop the capability to analyze and predict the necessary data to model those metrics of interest. The developed model needed to provide thrust and fuel flow as a function of Mach number, altitude, and throttle setting. Engine dimensions needed to be predicted and provided to aerodynamic analysis to assess aircraft drag. The engine weight needed to be predicted as part of the overall aircraft empty weight. Additionally, the propulsion analysis must provide the necessary information to model the noise produced by the engine.

Research Approach

Much of the details for the propulsion model were described in the last report [14]. As a brief summary, the propulsion system models a mixed-flow turbofan (MFTF) engine cycle. The engine cycle performance is modeled using Numerical Propulsion System Simulation (NPSS), and the dimensions, flowpath and weight are modeled using Weight Analysis of Turbine Engines (WATE++). This report focuses on changes applied to the propulsion model over the last year. For further details on the propulsion model, the reader is directed to the report from previous years and an AIAA article [21].

Propulsion Performance: Model

Several updates have been made to the propulsion cycle model. The pressure losses in ducts were previously set as constant values. This was updated so that the duct losses now scale with the square of corrected airflow in the duct, as described by Walsh [15]. The mixer loss model was also updated to better account for losses due to mixing as the flow conditions at the mixer change with flight condition, throttle, and variable nozzle throat. This is important for the noise power-management, which will be explained in the Off-Design Analysis section. The mixer loss model is based on the works of Frost [16] and Zola [17] and accounts for momentum losses due to unequal total pressures on the bypass and core side, friction losses in the chute of the mixer, and incomplete mixing losses. The turbine mean-line analysis was updated to ensure a 50% reaction design. This was done to ensure consistency with the efficiency correlations used. The number of stages for all turbomachinery can be adjusted to ensure reasonable work-coefficients (i.e., pressure ratio per stage). Since part of the mean-line analysis allows varying the design speed of the shafts and the radii of the turbomachinery, the stresses on the blades can change. To ensure that the allowable metal temperature used in the cooling flow model was appropriate to the blade stresses experienced, a turbine creep life model was implemented that uses a Larson-Miller correlation to estimate the creep life of the blades, given the metal temperature and predicted stress on the blades.

Propulsion Performance: On-Design Sizing

Engine cycle analysis previously used throttle ratio, the ratio of design turbine inlet temperature to maximum turbine inlet temperature, as a means of varying the theta-break, the Mach number at which the engine becomes temperature limited. However, with the turbine-creep life analysis setting a reasonable blade temperature, it was desirable to vary the maximum (max) turbine inlet temperature to trade cooling-flow penalties with the performance benefits of a higher turbine inlet temperature. This meant that for a given range of throttle ratio, the range of design turbine inlet temperature would shift with max turbine inlet temperature. Additionally, it was possible to set a throttle ratio that would place the theta-break at a higher Mach number than cruise. Because the point of picking a theta-break is to control the thrust lapse at cruise, it was decided to size the cycle such that design turbine inlet temperature was varied to target a desired corrected fan speed (i.e. thrust lapse) at top-of-climb when operating the top-of-climb turbine inlet temperature at maximum turbine inlet temperature. This ensures that both the max turbine inlet temperature and the thrust lapse at top-of-climb can be varied in a manner that ensures a more reasonable range of top-of-climb thrust lapse. This process is enabled by the multi-design point setup which allows perturbing design point parameters to meet targets at other flight conditions.

Propulsion Performance: Off-Design Analysis

In the last report, we detailed two different power-management schemes that utilize the fuel flow and a variable nozzle throat control. The first was an efficiency approach, used throughout the majority of the flight, by holding a peak efficiency line on the fan as the thrust was reduced. The second method favored noise when reducing thrust and is used only for landing and takeoff (LTO) noise analysis. This works by initially decreasing thrust along the 100% speed line of the fan, resulting in constant airflow and a greater reduction in fan pressure ratio and therefore jet velocity. This approach results in significantly more airflow in the bypass duct, which increases the Mach number and extraction ratio at the mixer. The mixer

model described above enables capturing the performance losses as a result of using this power-management scheme. The noise power-management approach has been further improved by favoring lower fan speed over lower fan pressure ratio at low thrust. This was done to favor a reduction in fan noise, which is dominant during the lower thrust used at approach. The fan operating point is always constrained by limits on the mechanical actuation of the nozzle throat as well as stall margin limits.

Propulsion Weight

As mentioned earlier, the stress predicted by the flowpath model is used to determine the turbine rotor blade creep life, which enables setting a reasonable allowable metal temperature. This in turn allows varying the maximum allowable turbine inlet temperature, which affects the amount of cooling air required to maintain the desired metal temperature. Additionally, noise results showed a significant reduction in noise from the fan rotor-stator spacing variable. To avoid exploiting the benefits of increasing rotor-stator spacing, the flowpath model is updated to reflect the increases in the length and weight of the engine. Additionally, an efficiency penalty is imposed on the fan to reflect the pressure losses that would occur in the extended distance between the rotor and stator due to both end wall friction losses and rotor wake mixing.

Results

The propulsion system modeling described in this section supports the design space exploration described and explained in Task 5. The results shown in Table 5 and Table 6 are the propulsion cycle performance and geometry and weight for the selected design discussed in Task 5.

Table 5. Engine performance for current selected design.

Engine Metric	Aerodynamic design point M1.2/39kft/ISA	Top-of-Climb M1.7/55kft/ISA	Takeoff M0.3/SL/ISA+18F
Fan pressure ratio	2.17	1.92	2.17
Bypass ratio	3.21	3.58	3.21
Overall pressure ratio	25.49	20.77	25.42
Compressor exit temperature (T3) [R]	1,357	1,540	1,460
Burner exit temperature (T4) [R]	3,173	3,536	3,360
Turbine inlet temperature (T41) [R]	3,083	3,436	3,266
Corrected airflow at the fan face [lbm/s]	908.8	839.3	919.3
Percent of design corrected fan speed	100.0	94.5	100.0
Thrust [lbf]	10,415.6	6,757	32,143
Thrust specific fuel consumption TSFC $\left[\frac{\text{lbm}}{\text{lbf}\cdot\text{h}}\right]$	0.847	1.029	0.642
Nozzle pressure ratio	4.58	7.71	1.99
Jet velocity [ft/s]	2,003	2,396	1,481

Table 6. Engine geometry and weight for current selected design.

Engine Geometry Variable	Value
Fan diameter [in]	67.2
Inlet capture area [in ²]	3,401
Engine pod length [in]	438
Engine pod weight [lb]	11,464

Task 3 - Mission Analysis

Georgia Institute of Technology

Objectives

The objective of mission analysis was to synthesize and size the supersonic transport for a specified design mission. The top-level requirement for sizing the current SST was to cruise at Mach 1.7 carrying 65 passengers for 4,250 nmi.

Research Approach

As with previous work, Georgia Tech researchers leveraged the Framework for Advanced Supersonic Transports (FASST) modeling and simulation (M&S) environment to model the supersonic vehicles for this task. This framework is based on the Environmental Design Space (EDS). The goals of EDS and FASST are the same: to provide a modeling and simulation environment that enables tradeoffs and interdependencies among aircraft system-level metrics. The difference is that EDS was designed for subsonic aircraft; therefore, modifications were implemented to enable the modeling and simulation of supersonic aircraft. In the case of FASST, the system-level metrics of highest interest are the vehicle weight, design mission fuel burn, and LTO certification noise. The flow diagram for the FASST environment (Figure 12) shows the inputs, outputs, and interconnections between each discipline's analysis module in the modeling and simulation environment.

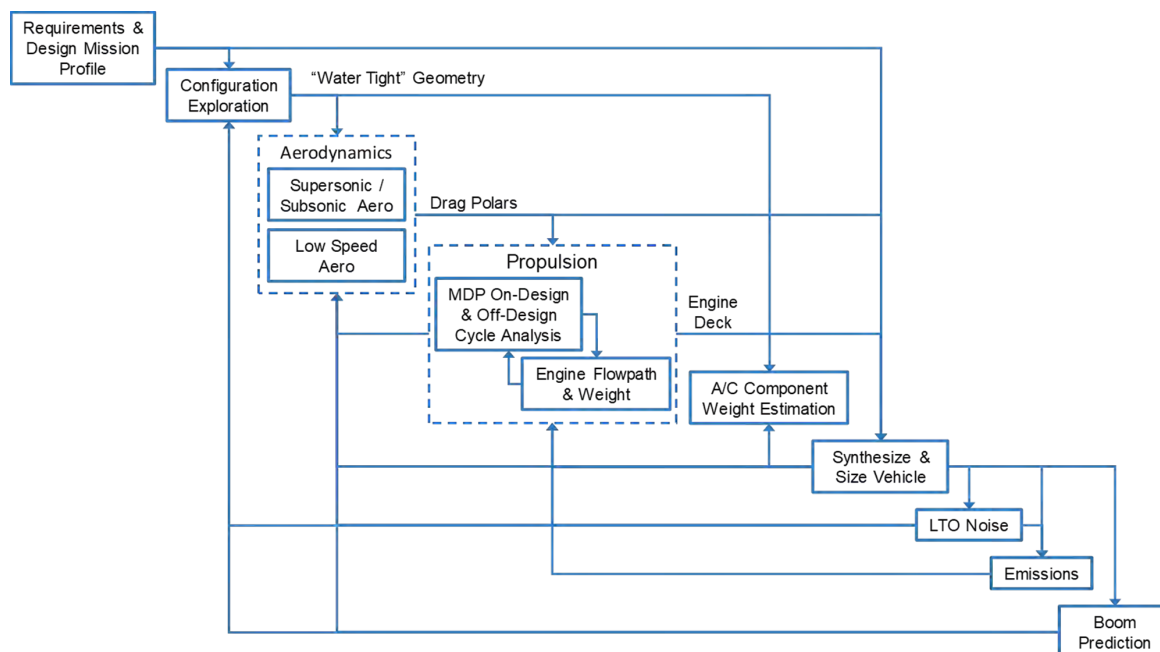


Figure 12. Framework for Advanced Supersonic Transport (FASST) flow diagram.

The requirements and design mission were specified by the research team and outlined in the following sections. Some of the high-level requirements were the number of passengers (65), the design Mach number (1.7), and the design mission range (4,250 nmi). The configuration exploration and aerodynamics drag polar generation are performed in a local setting, outside of FASST, and are described in Task 1. The resulting drag polars are fed into the mission analysis and vehicle sizing module. The engine cycle modeling is performed in NPSS, and flowpath and weight estimation is conducted with WATE. The engine architecture is a mixed-flow turbofan. The propulsion system modeling, discussed in Task 2, provides an engine deck, engine weight and engine dimensions to the mission analysis and vehicle sizing module. For the vehicle mission analysis and sizing, FLOPS is used. FLOPS uses the inputs of engine deck, drag polar, and other vehicle configuration parameters to estimate the overall empty weight of the aircraft. FLOPS then iterates on the vehicle gross weight to complete the mission prescribed by the designer. FLOPS also scales the engine thrust and wing area to produce the designer specified wing-loading and thrust-loading. If the engine is scaled in FLOPS, it is subsequently rescaled in the engine analysis to obtain an updated engine performance and weight. This iteration continues until the engine no longer requires scaling. After sizing, the vehicle is analyzed through a series of off-design missions.

Reference 18 offers more description of the mission segments within FLOPS; they are climb, cruise, refueling, payload releases, accelerations, turns, hold, and descent [18]. Many of these mission segments are developed for modeling military aircraft. The mission segments used for this study are climb, cruise, loiter, and descent, and the performance of each segment is done using a step integration method to compute fuel burn, elapsed time, distance covered, and changes in speed and altitude. The mission profile used for this study is shown in Figure 13. Also shown in Figure 13 is the reserve mission that is flown to compute reserve fuel. The reserve fuel has an additional safety margin of 5% of total trip fuel.

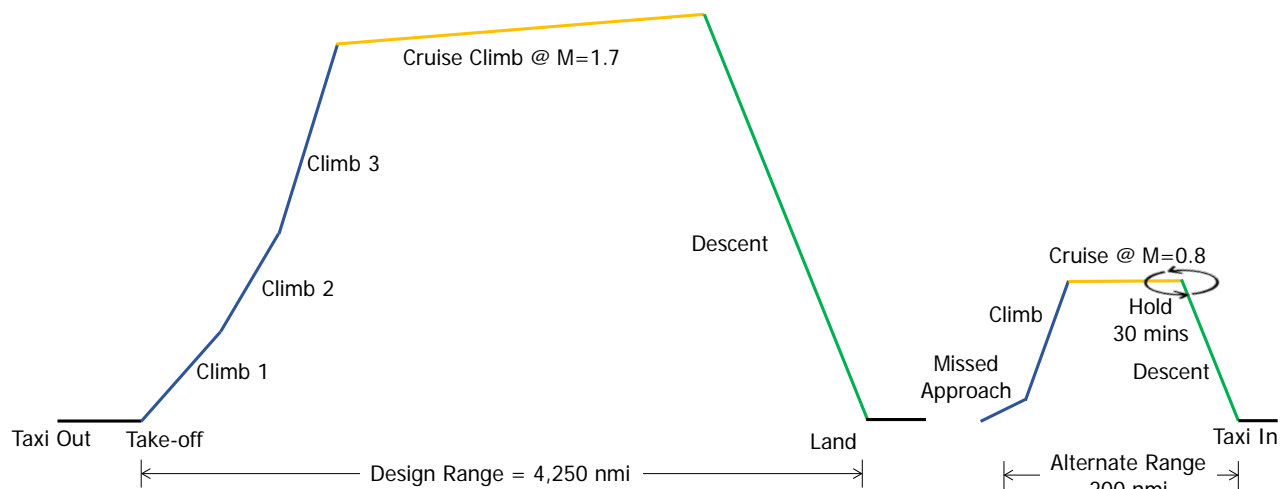


Figure 13. Mission profile for 65-passenger, M1.7 supersonic transport.

For the climb segment, FLOPS offers users a choice of providing a climb profile or it may be optimized by the program. The latter option is used for this sizing exercise. More specifically, the optimization option of minimum fuel to climb (as opposed to minimum time to climb or minimum time to distance) is chosen for the climb optimization. For this climb optimization, FLOPS divides the climb into a series of energy steps. Within each energy step, the combination of speed and altitude that maximizes the objective—in this case, inverse of minimum fuel—is determined.

For the cruise segment, FLOPS has several options for suboptimization, and they are optimum altitude, optimum Mach number, or both to achieve max specific range or minimum fuel flow, fixed Mach number and altitude, fixed altitude and constant lift coefficient, and maximum Mach number for either fixed altitude or optimum altitude. For the 65-passenger Mach 1.7 SST, the option of fixed Mach number/optimum altitude for specific range is chosen.

For the descent segment, FLOPS offers three options: prescribed profile, at constant lift coefficient, or at maximum L/D. For the SST of interest, the descent is flown with maximum L/D.

Although not part of the synthesis and sizing process, the detailed takeoff and landing module of FLOPS is used in order to provide detailed information on the takeoff and landing trajectories for the LTO noise analysis. The LTO noise prediction is discussed in the next task (Task 4 - LTO Noise Modeling).

Finally, to synthesize and size the supersonic transport, FLOPS requires the following information:

- Geometry definition of the optimized shape configuration from Task 1: Aerodynamics
- Parametric high speed drag polars from Task 1: SST Aerodynamics Modeling
- Landing and takeoff drag polars also from Task 1: SST Aerodynamics Modeling
- Engine deck, engine weight, and max nacelle diameter and length from generated from Task 2: SST Propulsion System Modeling
- Aircraft component weights from FLOPS internal empirical weight equations based on vehicle gross weight and geometric information provided
- Two major vehicle scaling parameters, wing loading (W/S) and thrust to weight (T/W) ratio, are varied with each mission analysis execution to satisfy balanced field length and approach speed constraints while minimizing take-off gross weight.

Results

The mission analysis result for the Mach 1.7 SST carrying 65 passengers for 4,250 nmi (excluding reserve mission) is listed below and depicted in Figure 14:

- Takeoff: Mach = 0–0.30 at altitude of 0 ft
- Subsonic climb: $M = 0.30\text{--}0.95$; altitude changing from 0 ft to 25,000 ft
- Transonic supersonic climb: $M = 0.95\text{--}1.4$; altitude changing from 25,000 ft to 30,000 ft
- Supersonic climb: $M = 1.4\text{--}1.7$; altitude changing from 30,000 ft to 47,910 ft
- Cruise climb: constant cruise $M = 1.7$; altitude changing from 47,910 ft to 54,771 ft
- Descent: deceleration from $M = 1.7\text{--}0.30$; altitude decreasing from 54,771 ft to 0 ft

The reserve mission results are as follows:

- Reserve fuel available: 28,139 lb (includes 5% of fuel used in main mission)
- Total hold time: 30 min
- Climb: from 0 to 30,000 ft, with Mach increasing up to 0.88
- Cruise: 30,000 ft at $M = 0.88$

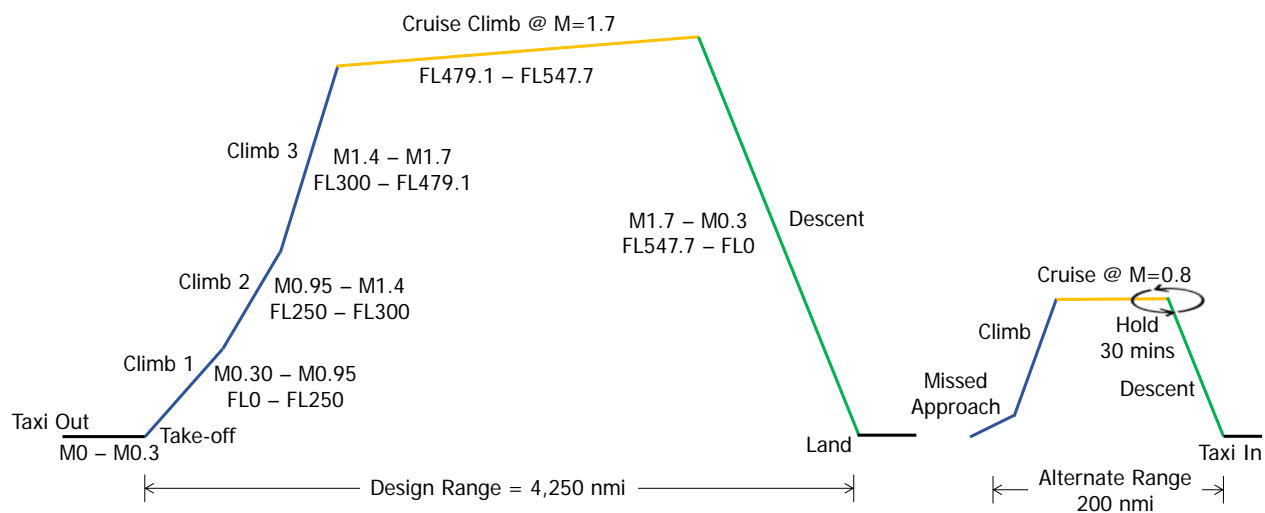


Figure 14. Mission profile for medium supersonic transport.

Task 4 - LTO Noise Modeling

Georgia Institute of Technology

Objective

The objective of this task was to study the impact of different takeoff trajectories and noise assessments for LTO noise. Alongside the team's traditional VNRS trajectory and its associated variables, the Georgia Tech group took upon the modeling of noise abatement departure procedures (NADP) set forth by NASA and ICAO, again with respective associated trajectory variables. Furthermore, in the interest of quantifying noise reduction benefits both close to and distant from the aerodrome, the team considered a new metric based on integrated sound exposure level (SEL).

Research Approach

As for many tasks developed by the Georgia Tech team in the context of supersonic aircraft, the modeling and simulation was performed in the FASST. Within this framework, once the configuration is properly modeled, the code uses FLOPS' detailed takeoff and landing module to calculate the takeoff trajectory. This information, along with many other engine and aircraft modeling parameters, is then passed on to ANOPP, which is also developed by NASA. The focus of this task is, therefore, to study the impact of the variables that control the takeoff trajectory on the noise assessment for a particular configuration. In essence, while this work is "nested" in the overarching design space exploration, the trajectory variables can be varied with no sizing impact to the configuration being studied.

The previously mentioned VNRS consists of a series of pilot-initiated and automatic (i.e., no pilot control) changes to engine and airframe configurations during a takeoff run to help reduce noise. In addition to the VNRS trajectory, two NADP trajectories, identified as ICAO-A and ICAO-B, have been implemented into the off-design analysis to explore other potential takeoff procedures. The ICAO-A trajectory is meant to minimize noise near the aerodrome and the ICAO-B trajectory is meant to minimize noise farther away from the aerodrome. To better illustrate each takeoff procedure, Table 7 presents a rundown of each of the options. Also, it is worth pointing out that the programmed high lift devices (PHLD) mentioned in Table 7 consist of a flap deflection schedule optimized for the aerodynamic efficiency for the required lift at each point in the takeoff trajectory, which is controlled by the flight management system. On a similar note, the programmed thrust lapse rate (PLR) is used differently by the VNRS and NADP procedures. In the former, it is an automatic thrust reduction controlled by FADEC and implemented immediately after the aircraft clears the obstacle during takeoff; in the latter, it is used as the engine cutback setting. Finally, the various highlighted aspects of each takeoff procedure are variables in our DoE that control aspects of the trajectory.



Table 7. Trajectories breakdown.

	VNRS	NADP-1 (ICAO-A)	NADP-2 (ICAO-B)
Takeoff start	Initiate the takeoff run with a specified power reserve (VARTH)		
After the obstacle	Reduce power to specified lapse (PLR), engage PHLD schedule and adopt a constant flight path (GFIX) and fly up to specified altitude (HSTOP_1)	Maintain current flight setting and fly up to specified altitude (HSTOP_1a)	Keep current thrust setting constant, adopt a constant flight path (GFIX_1b) and fly up to specified speed (VSTOP_1b)
	Transition to constant thrust and constant speed and fly up to specified altitude (HSTOP_2)		Engage PHLD schedule and fly up to specified speed (VSTOP_2b)
Pilot-initiated cutback	Cutback engine setting set automatically by FLOPS	Cutback engine setting set by the PLR variable in the next step	
		Transition to constant thrust and speed, reduce power to specified lapse (PLR) and fly up to specified altitude (HSTOP_2a)	Transition to constant thrust and speed, reduce power to specified lapse (PLR) and fly up to specified altitude (HSTOP_3b)
		Transition to constant thrust and flight path (GFIX_3a) and fly up to specified speed (VSTOP_3a)	Transition to constant thrust and flight path (GFIX_4b) and fly up to specified speed (VSTOP_4b)
		Adopt a constant flight path (GFIX_4a), engage the high lift devices schedule and fly up to specified speed (VSTOP_4a)	
Final segment	Fly off the aerodrome (50,000 ft distance from break release) with the previous settings		

As previously stated, the noise assessment for each aircraft configuration is done using NASA's ANOPP program. In performing these assessments, some assumptions were made in selecting and using different ANOPP modules. Table 8 presents a breakdown of the ANOPP input file structure and the rationale applicable to each module or section.

Table 8. Modules used in aeroacoustics analysis.

Component	ANOPP Module	Acronym	Rationale
Trajectory	Source Flyover Module	SFO	Considered separate trajectories (prescribed by FLOPS) for the sideline and the cutback/approach noises assessments – the difference being that the sideline trajectory did not include a cutback section after the second segment acceleration – and both cases used a VNRS takeoff trajectory
Airframe	Fink's Airframe Noise Module	FNKAFM	Standard module to predict the broadband noise from the dominant components of the airframe and based on a method developed by Fink for the FAA
Jet	Single Stream Circular Jet Noise Module	SGLJET	The single stream jet mixing noise was calculated with a methodology based on SAE ARP 876 as this is known to be the best representation of the current nozzle type
Fan	Heidmann Fan Noise Module	HDNFAN	The fan inlet and discharge noises were assessed separately for their tone and broadband contributions using a methodology based on correlations to model and full-scale test data
Treatment	Fan Noise Treatment Module	TREAT	Given that the chosen fan module assumes that the inlet and discharge ducts are without acoustic treatment, the attenuation spectra are applied to separate predictions of the inlet and aft radiated source noise produced by the source noise module and a total attenuated fan noise prediction is produced
Combustor	Combustion Noise Module	GECOR	The combustor noise was predicted with a methodology developed by General Electric, and later adopted by the SAE A-21 Committee
Shielding	Wing Module	WING	Used to compute the geometric effects of wing shielding or reflection on the propagation of engine noise (depending on the engine placement/configuration)

Finally, the key metric of merit for the LTO analysis for design/cycle selection is certification EPNL (effective perceived noise level), Georgia Tech has been starting to explore the potential for alternative noise metrics that better account for the whole noise footprint of the aircraft. While the most obvious means to do this would be to measure the noise footprint as predicted by AEDT, Georgia Tech currently does not have an automatic FFAST to AEDT pipeline, which would be needed to include AEDT results in our design space studies. For this reason, a new noise metric was considered where SEL was integrated along the flight path. Potentially this could be a more holistic method of comparing takeoff noise impacts, as opposed to only examining the three certification points, and better minimize noise footprints in a region of interest. By using this metric in combination with the ICAO-A and ICAO-B takeoff procedures, the Georgia Tech team plans to explore whether our current design space exploration procedure is optimizing for certification noise to the detriment of the overall noise footprint.

Results

Certification noise is a key metric for the design space exploration in described in Task 5, and the procedures described in this section allow the Georgia Tech team to analyze how this metric varies across the design space.

Task 5 - Design Space Exploration

Georgia Institute of Technology

Objective

The objective of this task was to explore a large design space of engine, airframe, and operational parameters to assess the interdependencies of fuel burn and LTO noise. In conceptual design, the final performance and environmental impact of a given vehicle is unknown. A key task in conceptual design is to parameterize the vehicle model such that different vehicle designs can be generated and evaluated. Doing so allows an assessment of how different parameters affect the metrics of interest and what the tradeoff between metrics looks like. By understanding these tradeoffs in the context of current regulatory limits, it enables designers to better understand how to design vehicles to meet current regulations and it allows policy makers an understanding of the implications of modifying current regulatory limits.

Research Approach

All the modeling elements described above and in previous reports are part of a modeling and simulation environment called FASST. FASST was used as the model to map alternatives to objectives. Alternatives were determined from a design of experiments, which included engine cycle, engine flowpath, thrust-loading, wing-loading, and LTO operational parameters. The engine cycle parameters include fan pressure ratio, overall pressure ratio, design turbine inlet temperature, max turbine inlet temperature, and extraction ratio (i.e., bypass ratio). The engine flowpath parameters include variables such as hub-tip ratio, tip Mach number, specific flow, etc. The LTO operational parameters include takeoff thrust setting, programmed lapse rate, second segment flight path angle, fixed-speed transition altitude, and cutback altitude. The design space exploration for the airframe geometry was done separately and described above in Task 1. From the available parameters, a DoE was used to generate alternatives. The design included a fractional factorial design and a random uniform sampling of several thousand additional designs. This was done as more sophisticated space-filling designs would take too long to generate given the number of designs desired. Additionally, the run time of FASST is fairly short and FASST can be distributed across ~1,700 cores using HTCondor [19]. The results are analyzed and plotted using JMP v16 [20], and ranges are refined for subsequent analysis as needed.

Results

Interim results of this work resulted in paper published at AIAA Aviation 2022; interested readers are encouraged to consult that paper [21]. This section will focus on the current status of results, which includes several model updates since the publication of that paper. These results pertain to a 65-passenger aircraft designed for a Mach 1.7 cruise and a range of 4,250 nmi. The results shown in Figure 15 demonstrate the type of results that can be obtained using FASST. The Pareto front is shown in pink and the currently selected design in green. These results are preliminary and require refining design variables ranges, as mentioned earlier, to fully resolve the Pareto front. Currently the Pareto front is not a smooth curve and appears to be missing designs at the lower noise margin. As such, additional runs will be performed to better resolve these trends. In identifying the Pareto front shown below, various constraints were imposed. These included limits on the takeoff and landing field lengths, approach speed, turbine creep life, and turbomachinery loading, as well as ensuring that each of the individual noise margins meets Chapter 14 requirements.

Additionally, obtaining these results involved increasing the empirical weight factors in FLOPS by 10%. There remains uncertainty in the applicability of current empirical correlations for a commercial supersonic transport. Although various items such as fuselage are expected to be greater due to the larger pressure differential at the higher cruise altitude and the higher dynamic pressure experienced by the airframe as a whole, there remains uncertainty as to what the weight of different parts of the aircraft will be. This will ultimately affect the results of the tradeoff shown below.

The results shown below are for a vehicle designed to cruise at Mach 1.7. In addition to the Mach 1.7 aircraft, a Mach 2.0 and Mach 1.4 vehicle will be evaluated in order to demonstrate how the interdependency shifts with Mach number. As Mach number is perhaps the most important design variable for a supersonic aircraft, it is important for policy makers to understand the implications of changing Mach number on this interdependency. Similarly, the upcoming results will inform designers when selecting the cruise Mach number for a vehicle.

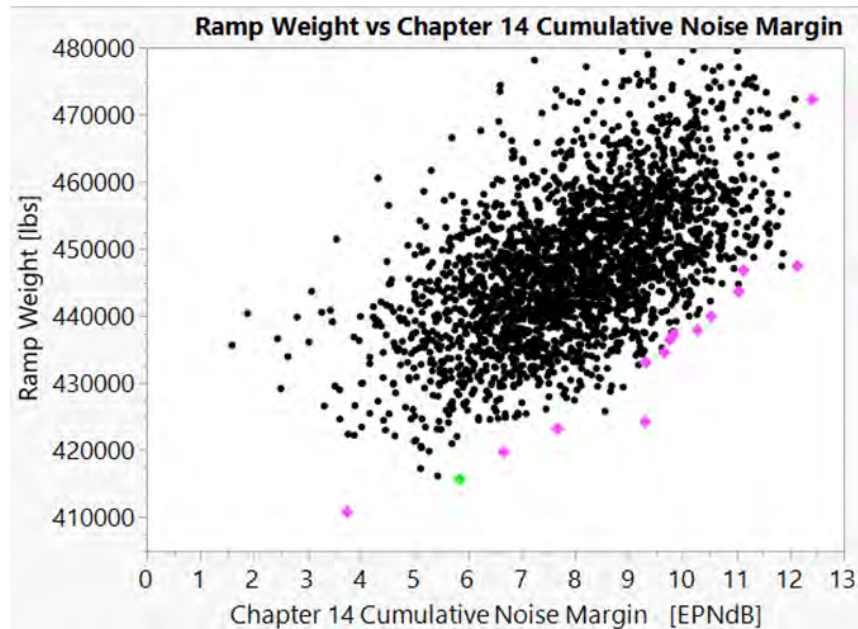


Figure 15. Pareto front of ramp weight vs noise margin.

Task 6 - SST Modeling in AEDT

Georgia Institute of Technology

Objective

The primary objective of this task is to propose a methodology for the construction of models to predict fuel burn, net thrust, and the drag coefficient value over the entire span of missions that a given SST will be performing and to support the implementation of full-flight modeling capability for SSTs in AEDT. A sample data package for the NASA Supersonic Technology Concept Aeroplanes (STCA) concept has been sent to FAA subject matter experts to kick-off the implementation efforts in AEDT on a set of four origin-destination (OD) pairs.

Research Approach

The technical approach for this section of the report is organized into propulsion data and aerodynamic data regression subsections. Also note that the propulsion and aerodynamic data used in this task are from a different SST discussed in Tasks 1 to 5 due to their availability.

Propulsion

To generate coefficients for net thrust and fuel consumption for each SST concept, the engine deck data are regressed using a fifth-order least squares linear regression through JMP. In this case, net thrust and fuel flow are both regressed against static pressure ratio, total temperature ratio, Mach number, and power code (δ_s , θ_t , M , and PC , respectively). This results in two regression equations with 31 coefficients (the unknowns) plus the intercept. For the sake of simplicity and efficient implementation within AEDT, note that both net thrust and fuel flow have the same regression equation form.

Because it is not possible to obtain a good fit for the whole engine deck data using one regression equation, boxes of different Mach number, altitude, and power code interval combinations are designated in such a way that the union of the set of boxes encapsulates the design mission and other notional missions for the specific SST concept in question. The data from the engine deck are then filtered according to these boxes, and the regression exercise explained above is employed for each box, resulting in two regression equations, one for net thrust and one for fuel flow, for each designated box. Shown in Figure 16 is the box selection for the 55-passenger M 1.8 SST concept, with the box selection for the ascent phase of the design mission in green and the descent phase in blue. In this case, 7 boxes would result in 14 equations. Also note that

the box selection is unique for each SST concept, because each concept has a different design mission. A concept with a higher cruise speed and altitude might require more boxes to be defined to obtain good regression results than would a concept with lower cruise speed and altitude.

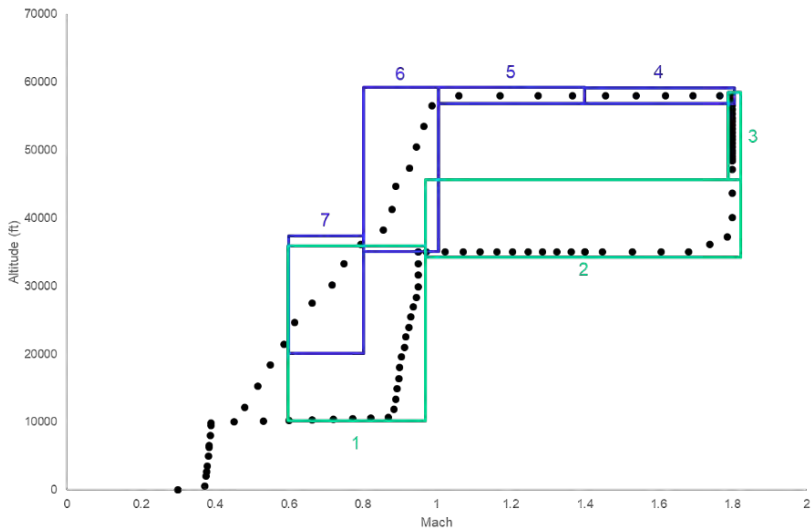


Figure 16. Propulsion box selection for 55-passenger M1.8 supersonic transport concept.

To evaluate the goodness of fits for each box, the values for predicted value for net thrust and fuel flow that can be obtained using the regression equations and the values for net thrust and fuel flow from the concept engine deck are used to calculate percent error. Probability density function distributions are then constructed using JMP to visualize the error for each box individually. A standard deviation of less than 1, a mean equal to 0, and percent error values lower than 4% at the 97.5% and 2.5% quantiles are all signs of a good regression. An example of these percent error distributions is shown in Figure 17.

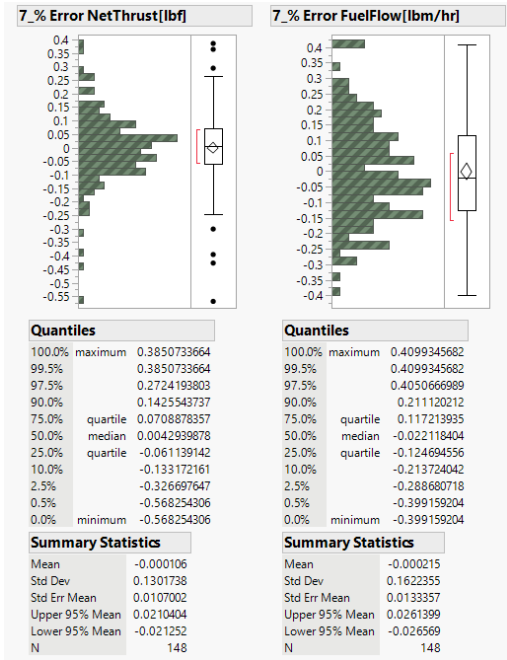


Figure 17. Percent error distribution example.



After obtaining a promising set of regressions for a particular concept, the next step is to validate them against the concept's design mission and off-design mission data generated using FLOPS. This will be explained in more detail in the validation section below.

Aerodynamics

To generate coefficients for the regression of the coefficient of drag for each SST concept, the design team provides raw FLOPS data that contain cardinal values of Mach number, C_L , altitude, and their corresponding C_D . The strategy that is exploited is to first regress the drag coefficient on those cardinal values using a stepwise fit before conducting a quadratic interpolation. By using this strategy with fewer C_L cardinal values, introducing Mach number as a cardinal value, and empowering the quadratic interpolation rather than the stepwise regression, the results were much better (errors ranged between -1.4% and 1.8%). Hence, the team decided to exploit this strategy for all future aero regressions using the latter strategy with fewer C_L .

JMP is exploited to perform the stepwise regression of the drag coefficient on Mach number, altitude, and C_L number. Because the behavior of the drag coefficient is quite different between subsonic, transonic, and supersonic phases, three different boxes are usually created and regressed against. The set of cardinal values to be chosen should always encompass the design mission in order to avoid extrapolation. Figure 18 shows an example of a supersonic regime equation obtained with the stepwise fit analysis.



Figure 18. Form of the equation yielded by the stepwise fit on the cardinal values of Mach number (green) and lift coefficient (C_L ; yellow) and a continuous altitude.

The design mission to which the validation is performed does not have specific cardinal values: Mach number, altitude, and C_L number are continuous. To enable predictive power for any input combination that is in between the original cardinal values of the inputs, a custom-made Python script was developed to perform a quadratic interpolation. The quadratic interpolation has the following form (see Figure 19):

$$C_D = a_1 + a_2 h + a_3 h^2 + b_1 + b_2 h + c_1 + d_1$$

$$b_1 = \begin{cases} b_{1,1}, & \text{if } M = M_1 \\ b_{1,2}, & \text{if } M = M_2 \\ b_{1,3}, & \text{if } M = M_3 \end{cases} \quad b_2 = \begin{cases} b_{2,1}, & \text{if } M = M_1 \\ b_{2,2}, & \text{if } M = M_2 \\ b_{2,3}, & \text{if } M = M_3 \end{cases}$$

$$c_1 = \begin{cases} c_{1,1}, & \text{if } C_L = C_{L,1} \\ c_{1,2}, & \text{if } C_L = C_{L,2} \\ c_{1,3}, & \text{if } C_L = C_{L,3} \\ c_{1,4}, & \text{if } C_L = C_{L,4} \end{cases} \quad d_1 = \begin{cases} d_{1,1,1}, & \text{if } M = M_1 \text{ and } C_L = C_{L,1} \\ d_{1,2,1}, & \text{if } M = M_2 \text{ and } C_L = C_{L,1} \\ \vdots & \\ d_{1,3,4}, & \text{if } M = M_3 \text{ and } C_L = C_{L,4} \end{cases}$$

Figure 19. Form of the quadratic interpolation.

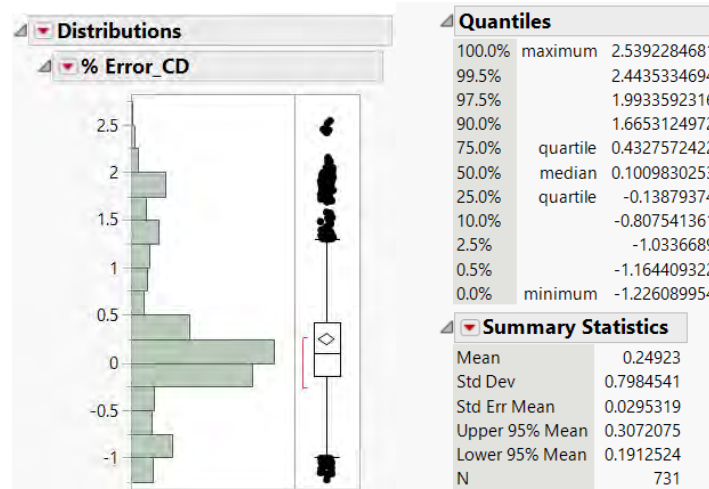


Figure 20. Total drag coefficient (C_D) error distribution example.

Figure 20 shows an example of total C_D error distribution after the quadratic interpolation has been conducted. Boxes are evaluated on their own at first, and then the total error distribution is evaluated. Once the fit is satisfactory, the design mission comes in and is considered as the validation set. This will be discussed in the next section.

Validation and Implementation in AEDT

The validation exercise consists of using the propulsion and aerodynamic regressions to obtain values for thrust, fuel flow, and drag coefficient for the SST concept's design mission and off-design mission data generated through FLOPS, and to compare the predicted values to the actual values from that data by calculating percent error and constructing probability density function distributions to visualize the results. To perform this exercise in a quick and efficient manner, a Python script was created that takes the propulsion and aerodynamic regression equations, as well as the data from the FLOPS mission, as inputs and calculates the percent error between the predicted regression outputs and the actual FLOPS outputs for net thrust and fuel flow. A flow chart that outlays how the validation process works and how the Python script was developed is shown in Figure 21.

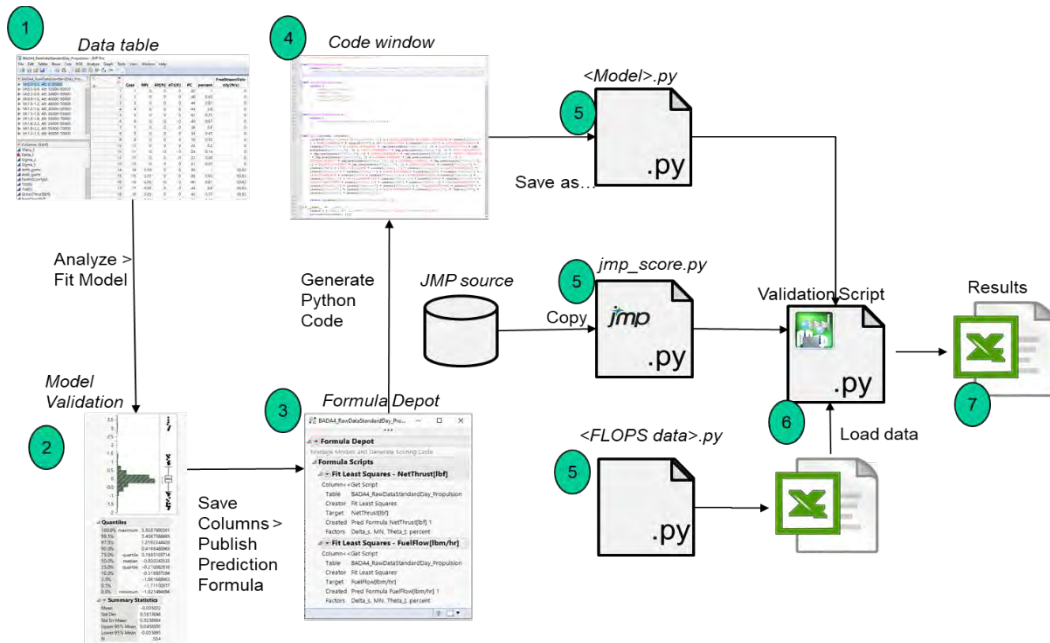


Figure 21. Validation process flowchart.

Since the FLOPS mission data does not contain values for static pressure ratio and total temperature ratio, atmospheric models must be incorporated into the code in order to calculate these values as functions of altitude and Mach number. Note that different models were used for the troposphere (altitude <36,089 ft) and stratosphere (altitude >36,089 ft) portions of the mission data to account for the differences in how static pressure ratio and total temperature ratio behave between the two regimes. The box selection used for the propulsion and aerodynamic regressions is also incorporated into the script, and the script automatically uses the corresponding regression equation for the segments of the mission data that fall into the designated boxes.

Assumptions That May Affect Modeling

The following assumptions about the atmosphere model, specifically for total temperature ratio and static pressure ratio, are made during the regression. The equations to compute the static pressure ratio are as follows:

$$\delta_s = \frac{P}{P_0} = (1 - 2.25577 \times 10^{-5} * h)^{5.25588} \quad \text{for altitudes below 11 km}$$

with P_0 = normal pressure at sea level (standard day) = 101,325 Pa

$$\delta_s = \frac{P}{P_0} = 1 + \frac{L_b}{T_0} \cdot (h - h_b) \cdot \frac{g_0 M}{R L_b} \quad \text{for altitudes above 11 km}$$

where

- P_0 = normal pressure at sea level (standard day) = 101,325 Pa
- T_0 = standard temperature at sea level [K]
- L_b = standard temperature lapse rate = -0.0065 [K/m]
- h = height above sea level [m]
- h_b = height at the bottom of atmospheric layer [m]
- R = universal gas constant = 8.31432 [N·m/mol·K]
- g_0 = gravitational acceleration constant = 9.80665 [m/s²]
- M = molar mass of Earth's air = 0.0289644 [kg/mol]

The equations to compute the static temperature ratio are as follows:

$$\frac{T}{T_0} = \delta_s^{\frac{L_b \cdot R}{g}} \quad \text{for altitudes below 11 km}$$

where

- δ_s = static pressure ratio
- T_0 = standard temperature at sea level [K]
- L_b = standard temperature lapse rate [K/m]
- R = universal gas constant = 8.31432 [N·m/mol·K]

For altitudes above 11 km, the static temperature ratio is assumed constant:

$$\frac{T}{T_0} = \frac{216.5}{288} = 0.751736 \quad \text{for altitudes above 11 km}$$

Using the appropriate static temperature ratio, the total temperature ratio is computed as follows:

$$\theta_t = \frac{T_t}{T_0} = \frac{T}{T_0} * (1 + 0.5 * (\gamma - 1) * M^2)$$

where

- γ = ratio of specific heats for a calorically perfect gas and has a constant value of 1.4
- M = Mach number
- T = static temperature at a given altitude [K]
- T_t = total temperature [K]

Input Data Format

For the first cut of the full-flight SST implementation in AEDT, the off-design missions for the NASA STCA are categorized into three classes: purely subsonic, purely supersonic, and mixed missions, and an OD pair was chosen for each of the categories. Table 9 lists the OD pairs and their airport (APT) IDs.

Table 9. Origin-destination pairs.

Mission Type	Departure APT	Departure APT ID	Arrival APT	Arrival APT ID
Purely Subsonic	VNUKOVO (Moscow)	11276	COTE D AZUR (Nice)	6052
Purely Supersonic	TETERBORO (Teterboro)	30540	FARNBOROUGH (Farnborough Military)	6570
Mixed	TETERBORO (Teterboro)	30540	BENITO JUAREZ INTL (Mexico City)	9457

The process for the off-design mission has two steps: ground tracking and route writing. Figure 22 depicts the flowchart that outlines this process.

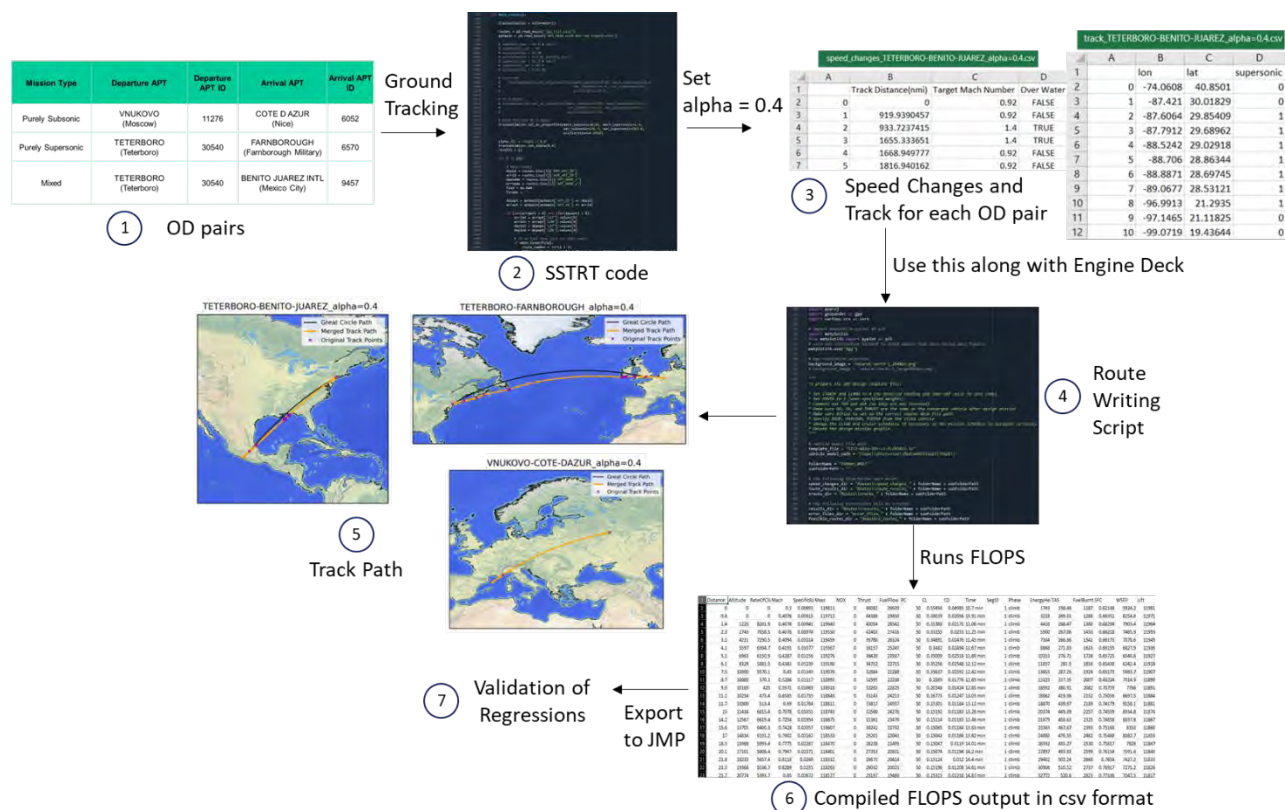


Figure 22. Off-design mission flowchart. OD, origin–destination; FLOPS, Flight Optimization System.

Validation of the Approach

Due to huge discrepancy between the predicted fuel burn by the model based on the engine deck compared with that given by FLOPS 8.11, a cumulative fuel burn sanity check has been performed on the A320neo. The results of this sanity check are shown below. The missions that were used to generate this will later be flown in AEDT, and the team will be able to finish the validation phase stating how accurate the proposed model is compared to the current AEDT model for subsonic aircraft.

Table 8. Propulsion validation.

Box	Actual Fuel Burn (lbm)	Predicted Fuel Burn (lbm)	% Error
Cruise/climb	33,563.56	33,322.35	0.719
Descent	515.53	514.66	0.168
TOTAL	34,079.09	33,837.01	0.710

Results

The JMP table generated from FLOPS output is used to validate the previously generated propulsion and aero regressions. The box definitions for these regressions are modified to reduce the % error based on the updated FLOPS data. Figure 23 and Figure 24 depict the modified box definitions for the propulsion and aero regressions, respectively. Table 10 and Table 11 tabulate the validation of the regression fits against the FLOPS outputs for propulsion and aero, respectively.

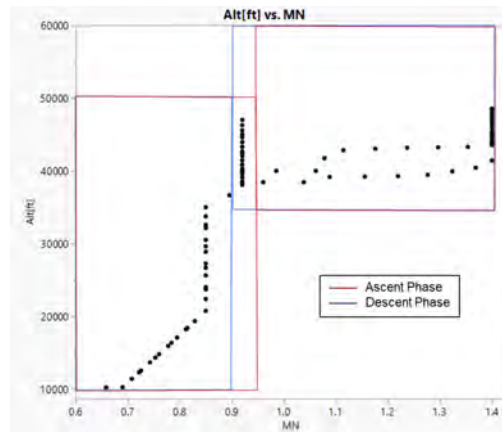


Figure 23. Propulsion box definition – NASA Supersonic Technology Concept Aeroplanes (STCA).

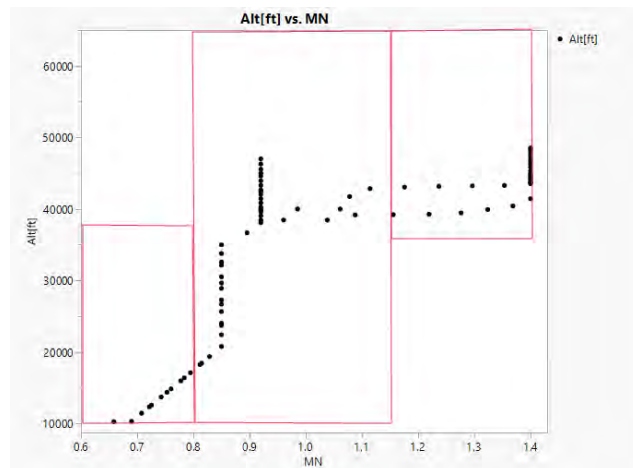


Figure 24. Aero box definition – NASA Supersonic Technology Concept Aeroplanes (STCA).

Table 10. Propulsion validation.

Box	Points per Box Training / Validation	Net Thrust				Fuel Flow			
		Training		Validation		Training		Validation	
		Mean	Std dev	Mean	Std dev	Mean	Std dev	Mean	Std dev
1	5,184 /119	-0.0070%	0.8786	-9.0027%	2.3982	0.0016%	0.5750	-9.9362%	1.5499
2	3,213 /40	0.0073%	1.2741	-5.8857%	3.6125	0.0047%	1.1494	-6.8557%	3.0681
3	1,020 /12	-0.0216%	1.2524			-0.0051%	0.5378	-0.9303%	1.0227
4	1,134 /48	0.0009%	0.4347			-0.0005%	0.2891	-4.3352%	1.3507

Table 11. Aero validation.

Mode	Points/Box	Training		Validation	
		Mean	Std dev	Mean	Std dev
Subsonic	72 / 36	0.0000%	0.0246	4.9182%	0.3294
Transonic	144 / 138	-0.0002%	0.1159	3.7639%	2.3807
Supersonic	84 / 33	0.0000%	0.0113	4.6703%	0.3037

The final data package consisting of the JMP table with the predicted formula of the net thrust, fuel flow rate, and C_D for each of the boxes have been provided to the FAA. The prediction formula can be exploited in diverse programming languages such as Python, C++, etc. to aid the implementation efforts in AEDT. Henceforth, the work will focus on supporting the implementation of the SST models and eventually developing full-flight modeling capability in AEDT.

Task 7 - Environmental Assessment Process

Georgia Institute of Technology

Objectives

The Georgia Tech team was tasked with supporting the EA of the planned SST testing by Boom Supersonic at Greensboro Airport. The process used by Georgia Tech to support this effort entailed the development of a generic SST that would be comparable to the planned Boom aircraft. Using the Georgia Tech FFAST tool, a design space exploration produced a field of aircraft that could be down-selected to a final configuration that met both Boom and FAA requirements for a notional SST to be used in the analysis for the EA. After the final vehicle was selected, acoustic analysis produced a set of noise power distance (NPD) curves, and trajectory analysis produced a set of fixed-point trajectories; both were imported into AEDT to produce a notional aircraft for use by the independent consultant hired by the FAA to conduct the EA.

Research Approach

Using the design process described previously in this report, the Georgia Tech team produced a field of potential configurations that could be used as the generic SST for the Greensboro EA as shown in Figure 25, which displays the filtered design space in terms of the MTOW over the Chapter 14 noise margin. Although Georgia Tech was able to generate a vehicle with up to ~7 dB margin to Chapter 14, the FAA requested that the Georgia Tech team select a vehicle with minimal noise margin to Chapter 14. The purpose of this was to analyze a more conservative vehicle in terms of noise performance, in case the test vehicle for the Greensboro airport underperformed Boom's predictions for noise margin. This would mean that the EA would be conducted using worse-than-expected noise emissions to provide a buffer for uncertainty in regards to the noise performance of this novel concept. The characteristics of the final down-selected vehicle are shown below in Table 12.

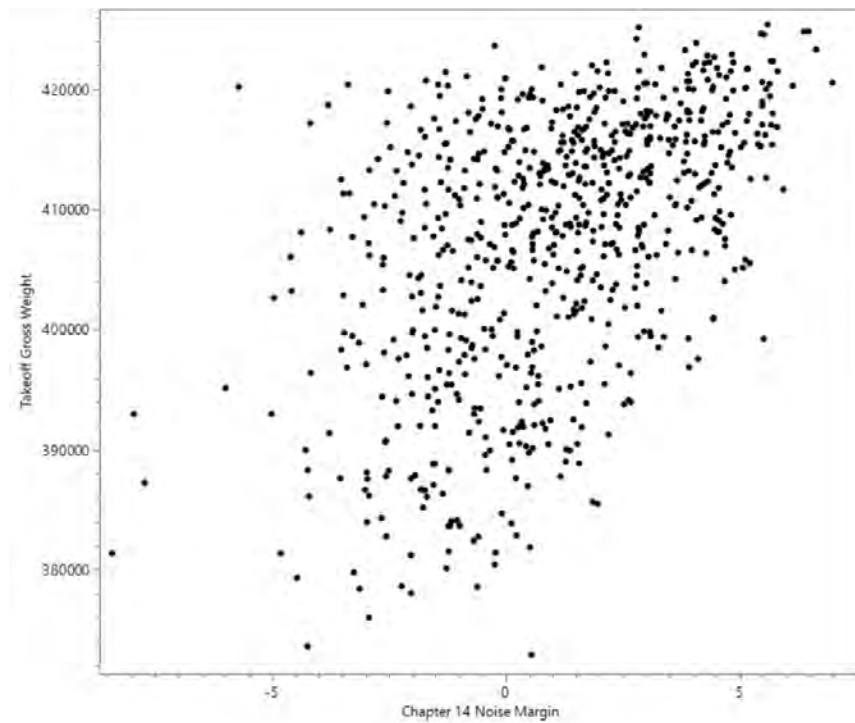


Figure 25. Design space exploration used for environmental assessment vehicle down-selection.



Table 12. Generic supersonic transport (SST) characteristics.

	Unit	Value
MTOW	Lbf	412,815
FPR (ADP, M1.2/39K)	Ratio	1.925
HPCPR (ADP, M1.2/39K)	Ratio	12.13
BPR (ADP, M1.2/39K)	Ratio	4.2429
Corrected mass flow @ fan face (ADP, M1.2/39K)	Lbm/s	1,108.04
Jet velocity	ft/s	1,168.37
TWR	Ratio	0.3366
WSR	Psf	88.498
Cutback noise	EPNdB	96.01
Approach noise	EPNdB	98.99
Sideline noise	EPNdB	92.83
Cumulative noise	EPNdB	287.83
Cutback margin	EPNdB	4.86
Approach margin	EPNdB	3.61
Sideline margin	EPNdB	6.34
Cumulative margin	EPNdB	0.81
Design range	nmi	4250
Far TOFL (OEO)	Ft	10,943.3
Landing field length	Ft	10,742.47

With a generic SST selected, three types of analysis are required in order to proceed with AEDT simulations: a weight-range study, fixed-point trajectory generation, and NPD generation. A requirement for AEDT is to define the stage length of a trajectory (since stage length serves as a proxy for aircraft takeoff weight in AEDT) and, because the test vehicle for the Greensboro airport currently plans to operate at 80% of its MTOW, it was necessary to ensure that one of the stage lengths defined in AEDT aligned with this MTOW percent. A weight-range study was conducted to discover the range that would correspond with the 80% MTOW target, and the results from this study are shown below in Table 13. This study revealed that a range of 2,422 nmi would correspond to the 80% MTOW target; therefore, stage length 4 was selected to represent this range in AEDT to serve as the proxy for the 80% MTOW configuration in AEDT, and the fixed-point trajectory for takeoff generated for AEDT was simulated with this takeoff weight in FLOPS. The output from the FLOPS simulation was selectively sampled to capture the shape of key aircraft trajectory parameters (altitude, ground track distance, thrust, and speed), while reducing the total number of data points required to ease database entry of the trajectory into AEDT. After this sampling of the FLOPS output was completed, a table consisting of horizontal distance relative to brake release, true airspeed (kts), altitude above field elevation (ft), and net corrected total thrust per engine (lbf) was compiled. All of these metrics are shown below in Figure 26. Similarly, this process was conducted for the approach trajectory for the aircraft's maximum landing weight. The trajectory information given to AEDT for approach is shown below in Figure 27.



Table 13. Generic supersonic transport stage length chart.

Stage Length	Range Interval (nmi)	Representative Range (nmi)	Weight (lb)	% Max Takeoff Weight
1	0-500	400	264,738	0.641
2	500-1,000	850	278,147.2	0.674
3	1,000-1,500	1,350	293,832.4	0.712
4	1,500-2,500	2,422	330,347.4	0.800
5	2,500-3,500	3,200	359,738.2	0.871
6	3,500-4,500	4,200	401,545.2	0.973

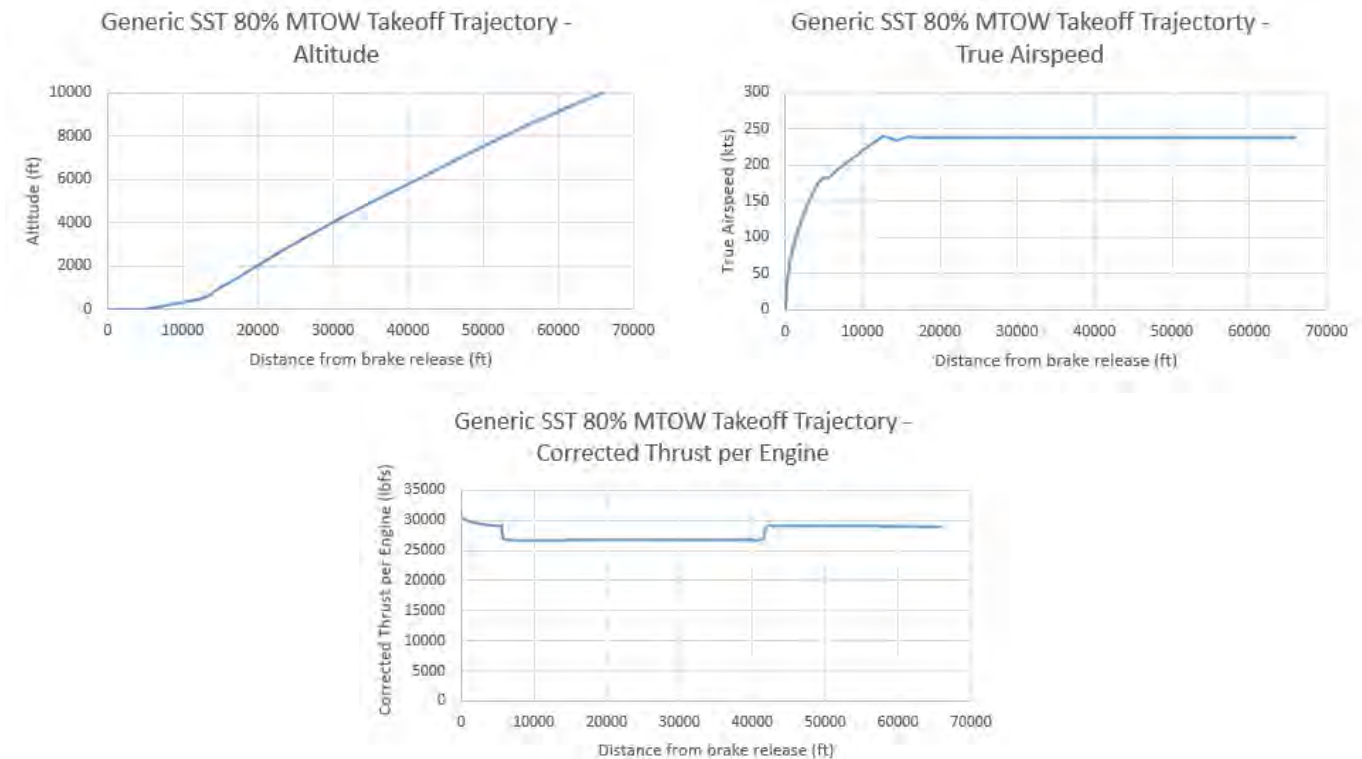


Figure 26. Generic supersonic transport (SST) 80% maximum takeoff weight (MTOW) takeoff trajectory.

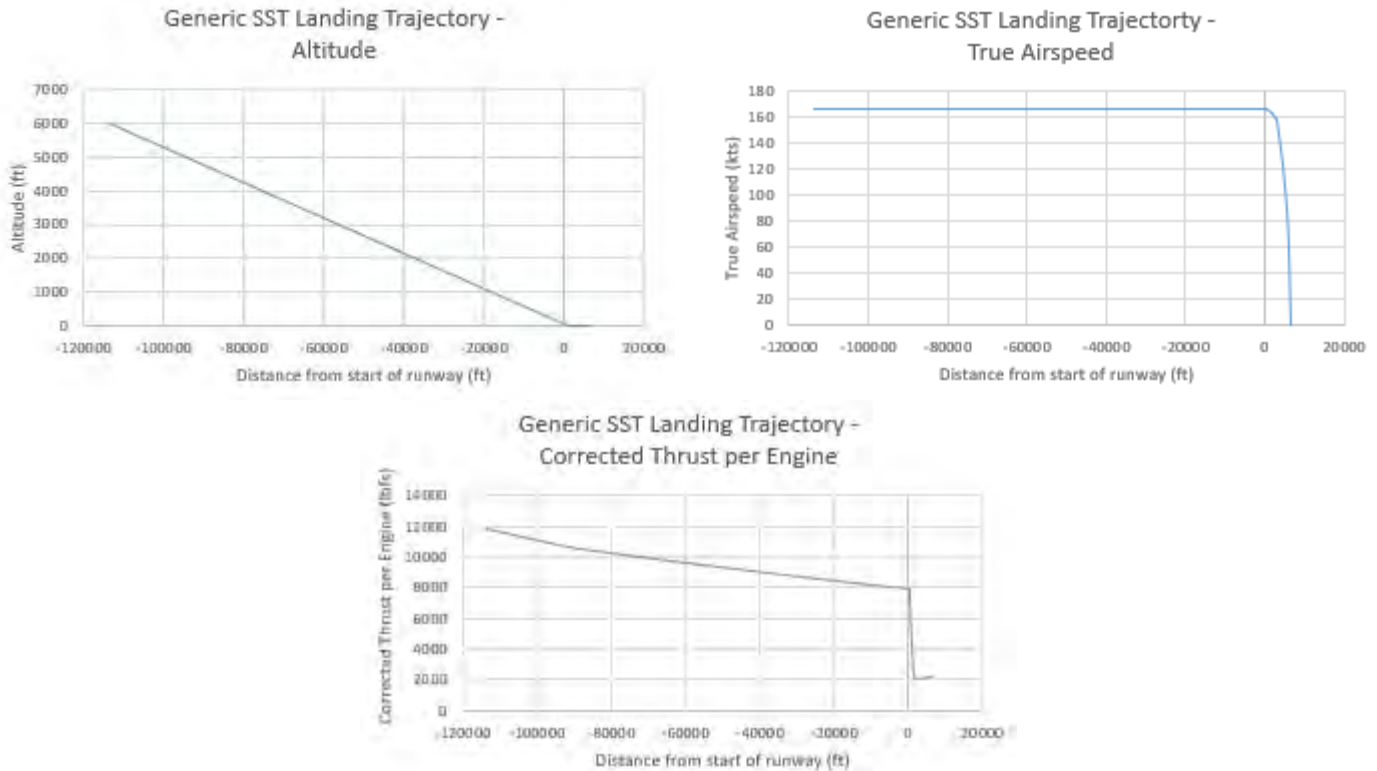


Figure 27. Generic supersonic transport (SST) landing trajectory.

NPD curves are a set of measurements from a single observer resulting from a series of steady level flyovers at various altitudes and throttle settings. NPD curves are expressed as four noise metrics: EPNL, SEL, maximum sound level (LAMAX), and perceived noise level tone-corrected maximum (PNLTM). The metrics that are used in this study will primarily be EPNL and SEL. The EPNL NPDs will be used in AEDT to verify that when the certification trajectory is simulated in AEDT, the predictions from AEDT for certification EPNL are within 1 dB of the ANOPP predictions to check consistency between the models. The SEL NPDs will be used to generation SEL noise contours, which will be one of the critical inputs when computing the area exposed to 65 dB day-night average sound level (DNL), one of the key parameters for the EA. NPDs along with the trajectories are included together in the dataset released to the FAA.

The other set of information the Georgia Tech team released to the FAA is an AEDT database updated to include the generic SST. The generic SST was included in the AEDT database by modifying an existing 777-200 aircraft file. Using the 777-200 ANP aircraft definition as a template, the NDPs, the fixed-point trajectories, and some key metadata information was updated to the values specified in the dataset described previously. Once this data had been updated, an AEDT model of the approach and takeoff certification trajectories was conducted, the purpose of which was to test whether the AEDT simulation predicted certification ENPL within the tolerance of 1 dB of the ANOPP predictions. The results are shown below in Table 14, indicating that there was agreement between the ANOPP and AEDT predictions.

Table 14. ANOPP and AEDT effective perceived noise level (EPNL) prediction comparisons (in EPNdBs).

	ANOPP	AEDT	Delta
Approach	98.99	98.93	0.06
Flyover/Cutback	96.01	95.49	-0.52
Sideline	92.83	92.02	-0.81

Results

The Georgia Tech team is supporting the Greensboro EA by providing aircraft trajectories, NPDs, and the AEDT database. The EA is ongoing at the time of writing; therefore, the Georgia Tech team will be refraining from publishing NPD dataset and SEL contour predictions. The Georgia Tech team intends to publish the team's findings once the ongoing FAA study has been completed.

Task 8 - Purdue Fleet Analysis

Purdue University

Objective

The Purdue team pursued four subtasks as a part of the fleet analysis task. During this year, the Purdue team developed cost estimation models for the acquisition and operating cost of the subsonic aircraft models, expanded the network of airline operations from the US-touching network to a global network, created simple sizing and performance models for alternate supersonic aircraft, and developed a demonstration model for the estimation of operations and emissions of business jet aircraft.

Subtask 1: Acquisition and Operating Cost Estimation Models

Previously, the aircraft cost information needed for FLEET simulations, including the acquisition and operating costs, were generated using the cost module of FLOPSv8. The cost module is no longer available in FLOPSv9, and a new cost model with similar functionality was needed. The cost model needs to provide the costs information needed for FLEET, so the team named this the FLEET cost function (FCF). The FCF categorizes the cost items in exactly the same categories needed as inputs to FLEET:

- Acquisition cost,
- Direct operational cost (DOC, which includes flight and crew cost, maintenance cost, aircraft servicing cost, and insurance cost), and
- Indirect operational cost (IOC, which includes ground property and equipment cost, passenger service cost, and other costs not directly related to flight service).

Note that, while the fuel cost is usually considered part of the DOC, FLEET considers this separately to study the impact of future fuel prices and/or prices for alternative or sustainable jet fuels. Therefore, fuel cost is external to FCF.

To build the FCF, four well-known cost models were used. For the acquisition cost, FCF uses a modified RAND DAPCA IV model from Raymer [22]. For operational costs, FCF uses a mixed model combining the Liebeck model [23], the ATA model [24], and a model originally developed by Johnson for FLOPS [25]. Although the different cost models mentioned have different baseline dollar years, all costs in the final version of FCF are converted to 2011 US dollars (USD) to reflect the newest starting year in the worldwide version of FLEET using a Consumer Price Index (CPI) inflation calculator from U.S. Bureau of Labor Statistics [26]. If the desired starting year of FLEET simulation is different from 2011, the CPI factor will need to be changed accordingly for all cost components. Using the CPI adjustment is straightforward and the information is readily available; not all aircraft-related costs will follow the CPI.

Acquisition Cost Model

A modified version of RAND's DAPCA IV model from Raymer's "Aircraft Design: A Conceptual Approach" (sixth edition) provided the acquisition cost estimation, and some calibration of this used previous FLOPS results and real-world data. Raymer's version of the DAPCA model was modified and converted to 2011 USD values. The DAPCA model mainly uses empty weight, maximum velocity, and the number of aircraft to be produced in five years as variables to determine the acquisition cost, among a few other variables that have less effect on the result. Because empty weight and maximum velocity are aircraft parameters that are an input (maximum velocity) and an output (empty weight) of the aircraft sizing code, the number of aircraft to be produced in five years (Q) is the variable to adjust in order to calibrate the acquisition price. The models and acquisition prices used for calibration appear in Table 15, based on the available FLOPS aircraft models previously tested. The historical acquisition price is mainly from Boeing's website [27], credible sources such as Jane's [28], and aircraft industry enthusiast websites such as <https://aerocorner.com/aircraft> [29]. For calibration, the acquisition price of the aircraft is assumed to be the same as the advertised or published value. Note that the listed price from those sources may be different from the actual price airline companies pay to the manufacturer, because there are almost always additional deals made

between manufacturers and airlines to bring the acquisition price lower than the listed or advertised price. Details of these discounts and actual sale prices are not publicly available.

Table 15. Aircraft models used for acquisition cost calibration.

Regional Jet	ERJ 145	CRJ 200	CRJ 700	CRJ 900
Acquisition cost [million 2005 USD]	20.68	24.00	32.10	32.00
Single-Aisle	B737-300	B737-700	B737-800	B757-200
Acquisition cost [million 2005 USD]	37.90	56.50	67.75	81.60
Twin-Aisle	B767-200ER	B777-200LR	B747-400	A330-200
Acquisition cost [million 2005 USD]	113.23	220.50	220.75	143.30

After testing and calibrations, a different value of Q is assigned to aircrafts of different sizes: for aircraft less than 100 seats in a two-class layout (regional airliner), Q is equal to 375; for aircraft larger than 100 seats but less than 200 seats in a two-class layout (single-aisle airliner), Q is equal to 210; and for aircraft larger than 200 seats in a two-class layout (widebody airliner), Q is equal to 165. The resulting acquisition price for the historical aircraft models in Table 15 is as shown in Figure 28.

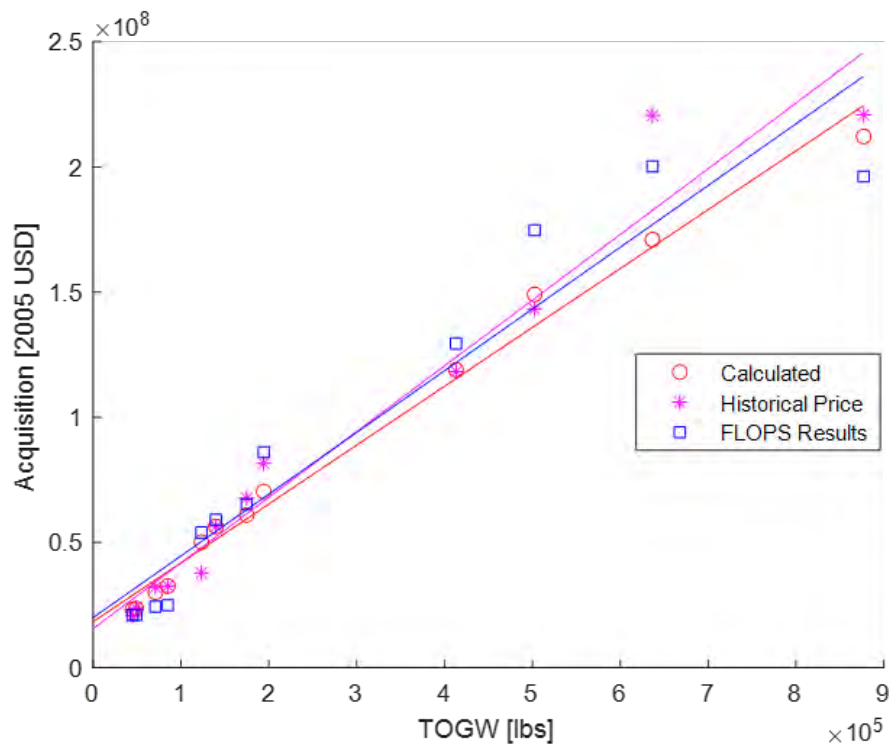


Figure 28. Acquisition prices for the historical aircraft models. FLOPS, FLight Optimization System; TOGW, takeoff gross weight.

Direct Operating Cost Model

The operational cost model is built with various models to have operational costs with a similar trend and scale as the previous operational costs predicted by FLOPSv8 with the limited input information. The Liebeck model [23] calculates the maintenance costs and pilot costs; the ATA model [24] calculates the insurance costs; and Johnson's model [25] calculates

the servicing costs and IOC. Note that, in theory, Johnson’s model should produce the same cost results or at least a similar trend compared with the current operational cost inputs to FLEET, which were generated by the cost module in the previous FLOPSv8. However, upon testing, the costs generated from FLOPSv8 do not always have a similar trend to the original version of Johnson’s model. Sometimes, Johnson’s model requires a significant number of additional inputs that the sizing code no longer uses and default input values that might have been used in the FLOPSv8 implementation were unknown to the Purdue team. As a result, the cost model for some cost components was chosen to be from Liebeck or ATA, which are well-known aircraft cost estimation methods.

The operational costs are calibrated using the previous results from FLOPSv8 to the same scale, because calibrating the costs to have the same trend is extremely difficult without knowing the equations used. The 2011 Bureau of Transportation Statistics (BTS) database Air Carrier Financial Report (Form 41) data [30] was used as a guideline to determine if the pilot salary, maintenance cost, and insurance cost estimations are reasonable.

The resulting operational costs have a similar scale and proportions to the previous cost input for FLEET. Figure 29 presents the resulted DOC (including fuel cost) and IOC for a Boeing 737-800 aircraft on a 2,950 nmi mission with the same payload and fuel burn/fuel cost. For the previous result from FLOPS, the total DOC (without fuel) is \$8,495, and the total IOC is \$22,252; for the result from FCF, the total DOC (without fuel) is \$9,144, and the total IOC is \$19,365, which has a total operational cost 7.3% lower. Notice that the difference in the resulting operational costs is model- and mission-dependent (i.e., the overall operational cost might end up being higher for some models but lower for other models on the same route), and the overall average difference in the operational costs is lower than 5%.

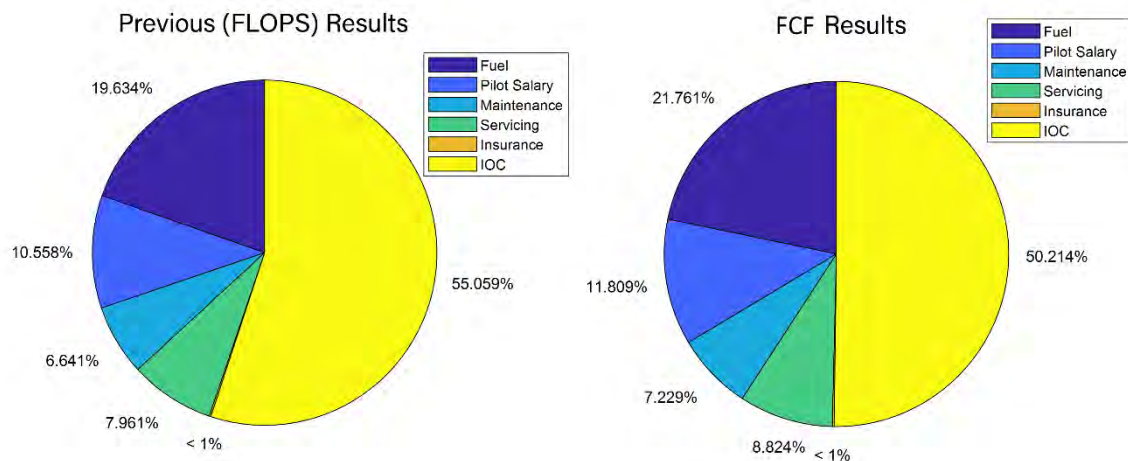


Figure 29. Operational cost for Boeing 737-800 at a 2,960 nmi mission. FLOPS, FLight Optimization System; FCF, FLEET cost function; IOC, indirect operating costs.

Subtask 2: Expand FLEET Route Network

Overview of Worldwide Demand Data and Representation

To extend FLEET’s capability to provide supersonic and subsonic aircraft allocation data on global routes (in addition to those present in the previous FLEET network of “US-touching” routes), the Purdue team updated FLEET’s route network to a worldwide route network. The global fleet demand data were obtained from the Official Airline Guide (OAG) Traffic Analyser [36]. The data were extracted from the OAG Traffic Analyser for years 2011 to 2020; OAG did not have relevant global fleet demand data available for any year earlier than 2011. Based on this global data availability, the team decided to move the initial year of FLEET simulation from 2005 to 2011 and update the initial network, passenger demand, and fleet composition accordingly.

In 2019 (and all subsequent years), there are 5,317 routes in the FLEET network that connect a subset of WWLMINET 257 airports. Comparing this with the previous “US-touching” route network in FLEET, this is a 170% increase in the number of



routes, increasing from 1,974 routes (US-touching only) to 5,317 routes (worldwide). Figure 30 compares the worldwide route network with the US-touching only network, visually highlighting the increased routes in the new network.

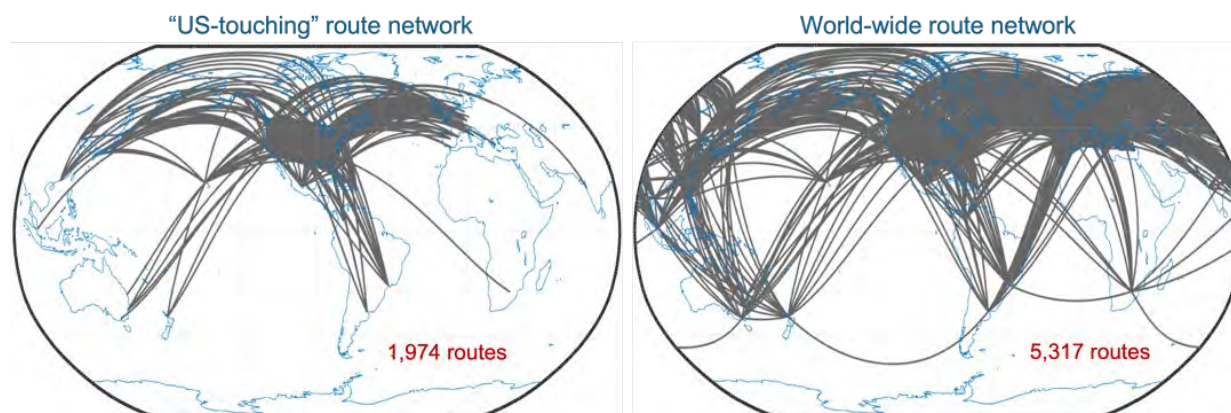


Figure 30. Comparing the worldwide route network with the existing US-touching route network in FLEET.

Estimation of Fleet Size and Mix for Worldwide Operations

The methods to determine the 2011 initial global fleet composition are similar to the methods described in Moolchandani's thesis [31] to obtain the 2005 initial US fleet. However, the methods have been adapted accordingly with expansion to include a global fleet instead of just the US fleet. BTS data of the 2011 US fleet was the primary source to determine the detailed fleet composition. Boeing's 2012-2031 Current Market Outlook Report [32] (hereafter called Boeing's) and Oliver Wyman's 2017 Global Fleet & MRO Market Forecast Summary [33] (hereafter called OW's) were used as the primary sources to determine the global fleet size in 2011. The resulting 2011 initial global fleet is shown below in Table 16. Details about the worldwide fleet geographic regions, representative model, how the initial fleet divided into representative-in-class and best-in-class models based on age, and the average age for each model is available at the end.

Table 16. 2011 Initial global fleet. RIC, representative-in-class; BIC, best-in-class.

	Africa		Middle East		Asia Pac		Latin America		North America		CIS		Europe		World	
	RIC	BIC	RIC	BIC	RIC	BIC	RIC	BIC	RIC	BIC	RIC	BIC	RIC	BIC	RIC	BIC
Class 1	20	230	0	40	40	370	20	220	140	1370	20	190	50	480	290	2900
Class 2	10	140	0	20	20	230	10	140	70	850	10	120	20	300	140	1800
Class 3	90	150	90	140	680	1080	220	350	830	1320	160	250	640	1010	2710	4300
Class 4	50	110	50	100	370	770	120	240	450	930	90	180	340	710	1470	3040
Class 5	20	50	90	200	200	470	10	30	150	360	20	50	120	280	610	1440
Class 6	10	30	30	140	60	300	0	10	40	210	10	30	30	160	180	880
Total	200	710	260	640	1370	3220	380	990	1680	5040	310	820	1200	2940	5400	14360
	910		900		4590		1370		6720		1130		4140		19760	

Regions in the Global Fleet Network

As shown in Table 16, the 2011 initial global fleet divides the global fleet into seven regions: Africa, Middle East, Asia Pacific, Latin America, North America, Commonwealth of Independent States (CIS; East Europe), and Europe. This follows the same geographic regions as in Boeing's. Although FLEET is not able to utilize any of this detailed information during allocation, it may be beneficial for future FLEET works when FLEET is capable of allocating aircraft separately in each geographic region. Figure 31 from Boeing's below shows the mapping of each region.



Figure 31, Global fleet regions.

Classification Method and Representative Models of Aircraft

Because detailed global fleet data were not widely available, the 2011 BTS data of the US fleet composition are used to determine the classification method and the representative models of aircraft operating in the new 2011 worldwide network. It is assumed that the model and age of aircraft in the US fleet is representative of the fleet in the rest of the world. This assumption may not be perfect, but given the available data, it is deemed adequate for the purposes of this work. The 2011 worldwide network is represented by 14 aircraft models, divided into six classes based on seat capacity, and then into representative-in-class (RIC), best-in-class (BIC), and new-in-class (NIC) based on the average age of the aircraft according to the BTS data. The previous classification and representative models in 2005 US-touching FLEET network are shown below in Table 17 as the starting point of the work.

Table 17. 2011 Classification of aircraft classes for US-touching network.

Class	Seats	Representative-in-Class	Best-in-Class	New-in-Class
Class 1	20 – 50	Canadair RJ200/RJ440	Embraer ERJ145	Aircraft X1
Class 2	51 – 99	Canadair RJ700	Embraer 170	Aircraft X2
Class 3	100 – 149	Boeing 737-300	Boeing 737-700	CS100
Class 4	150 – 199	Boeing 757-200	Boeing 737-800	Purdue ASAT
Class 5	200 – 299	Boeing 767-300	Airbus A330-200	Boeing 787
Class 6	300+	Boeing 747-400	Boeing 777-200ER	Aircraft X6

A few adjustments are made to the previous table. Previously, RIC were models with the greatest number of aircraft in the fleet; BIC were the models with the most recent service entry date; and NIC were models in development that will enter service in 2015. In the 2005 baseline year for the US-touching network version of FLEET, this classification made sense and could be a good indication of the average age and technology age of the models, where the RIC has older average age and technology age than the BIC (and NIC would be the newest in the fleet when entering service). In the BTS 2011 data, we found that for many aircraft seat classes, the models with the greatest number of aircraft in the fleet were no longer the “oldest” model. As a result, in the 2011 worldwide network, the RIC was the model with an average age >10 years; BIC were the models with an average age <10 years; and NIC were still the models that entered service in 2015. Note that for different classes, the dividing ages for RIC and BIC are different; more details will be shown in the later Age Distribution section.

As in the 2005 US-touching fleet, the six seat-capacity classes can roughly represent the different sizes of aircraft: Class 1 and 2 are generally regional jet/turboprop aircraft; Class 3 and 4 are generally single-aisle/narrow-body aircraft; and Class 5 and 6 are generally double-aisle/widebody aircraft. The six seat-capacity classes in the 2011 worldwide fleet were the same

as in 2005 US-touching fleet, except in Class 5 and Class 6. In the 2005 US-touching fleet, Class 5 has 200-299 seats, and Class 6 has more than 300 seats. In the 2011 worldwide fleet, Class 5 has 200-279 seats, and Class 6 has more than 280 seats. This change is primarily made to divide some large twin-aisle airliners (such as the Boeing 777 and Airbus A350) into Class 6 instead of Class 5. Based on the manufacturers' information, those large twin-aisle airliners can carry more than 300 passengers in two-class or even three-class configurations. As a result, they should be able to be classified as Class 6 aircraft in the 2005 US-touching network. However, in the 2011 BTS data, the researcher found that most of the Boeing 777s in the US operators had a seating capacity of around 290. The US operators configured the aircraft into a three-class configuration and potentially gave larger space for each seat to provide a better experience for transcontinental flights. The resulting representative models of each class are shown below in Table 18. Each model was the one with the greatest number of aircraft in the BTS data that fell into the specific seat-capacity range and average age range. Note the Class 1 will be discontinued in new and future-in-class models.

Table 18. Representative models and classification of 2011 worldwide fleet.

Class	Seats	Representative-in-Class	Best-in-Class	New-in-Class	Future-in-Class
Class 1	20-50	Saab 340B	CRJ-200	-	-
Class 2	51-99	ATR 72	CRJ-700	Gen 1 DD RJ (2020)	Gen 2 DD RJ (2030)
Class 3	100-149	MD 80	Boeing 737-700	Gen 1 DD SA (2017)	Gen 2 DD SA (2035)
Class 4	150-199	Boeing 757-200	Airbus A320-200	Gen 1 DD STA (2025)	Gen 2 DD STA (2040)
Class 5	200-279	Boeing 767-200	Airbus A330	Gen 1 DD LTA (2020)	Gen 2 DD LTA (2030)
Class 6	280+	Boeing 747-400	Boeing 777-200	Gen 1 DD VLA (2025)	Gen 2 DD VLA (2040)

Age Distribution

Because detailed global fleet information is not available to the team, an assumption was made that the global fleet in 2011 has the same class-wise age distribution as in the 2011 BTS data for the US fleet. This assumption may not be very accurate in some regions such as Asia and the Middle East. The fleets in those regions will likely be younger than the US fleets because airline fleets in those regions have grown rapidly in recent years and massive numbers of new aircraft were acquired. The resultant age distribution for each class is shown in Figure 32, with different presentation of the age distribution for each class.

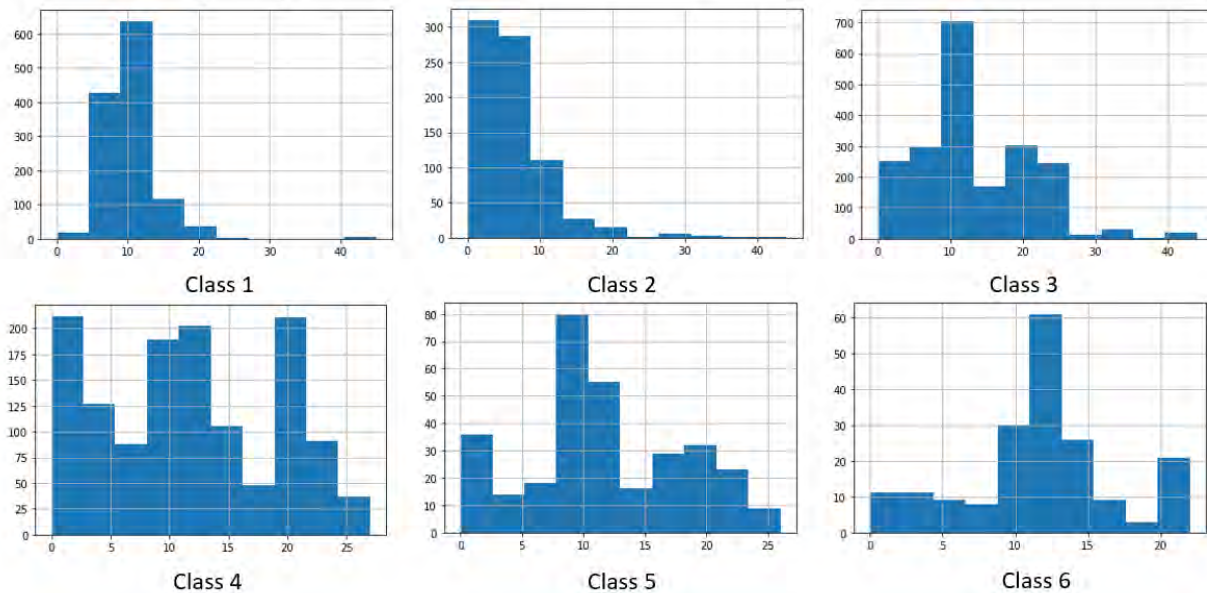


Figure 32. Age distribution (x-axis; years) in Bureau of Transportation Statistics (BTS) 2011 data for each class.

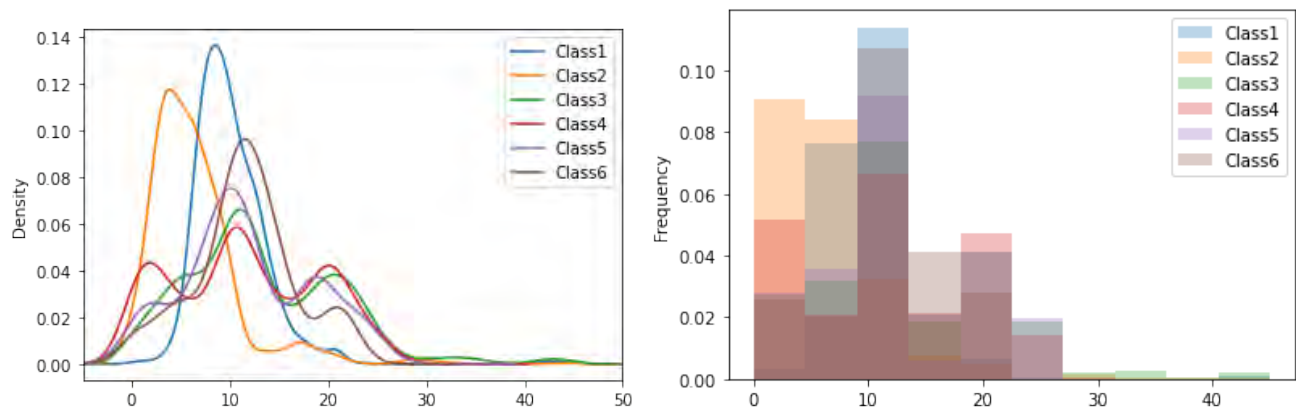


Figure 33. Age distribution in Bureau of Transportation Statistics (BTS) 2011 data for each class in percentage. Notice that the x-axis of the two plots is the age of the aircraft in years.

As the above figures show, the different classes have different age distributions. This indicates that the different classes of the fleet have very different age compositions and possibly very different technology age distributions. As a result, dividing the entire fleets to RIC and BIC based on only a single common factor seems unreasonable. Hence, we divided the average age for the RIC and BIC modes according to the BTS 2011 US fleet data, as shown below in Table 19. We can confirm that dividing ages were reasonable, as each average age for RIC and BIC lies around the peaks, as shown in Figure 33.

Table 19. 2011 US initial fleet divided into representative-in-class (RIC) and best-in-class (BIC).

Class	Dividing Age	RIC Mean Age	BIC Mean Age
Class 1	14	18.37	9.37
Class 2	12	19.39	5.30
Class 3	13	21.74	8.17
Class 4	15	20.43	7.40
Class 5	15	20.13	8.26
Class 6	15	19.52	9.87

FLEET Allocation Results for Worldwide Operations (Subsonic Only)

The results shown here consider the previously developed “Current Trends Best Guess” (CTBG) scenario (presented in previous annual report [34]) as the baseline scenario, utilizing the subsonic-only CTBG results on both the US-touching network and the new worldwide network for comparing and analyzing. Note the CTBG scenario presented here *does not* include the impact of the COVID-19 pandemic on air travel demand and is referred to as “baseline (no COVID)” scenario in later parts of this section. The FLEET simulations using the worldwide network ran from year 2011 to 2050. Figure 34a compares the normalized fleet-level CO₂ emissions considering a worldwide network (depicted by the solid red line) with the CO₂ emissions considering a US-touching only network (depicted by the solid blue line). As expected, the CO₂ emissions considering a worldwide network are always higher than those from the US-touching network due to the increased network size; in 2050, total CO₂ emissions for the worldwide network simulation are about 2.7 times higher than for the US-touching network. This increase in emissions is proportional to the increase in the network size (the number of routes increased from 1,974 to 5,317, an almost 2.7-fold increase), as the aircraft models used in the simulation are the same for the two route networks.

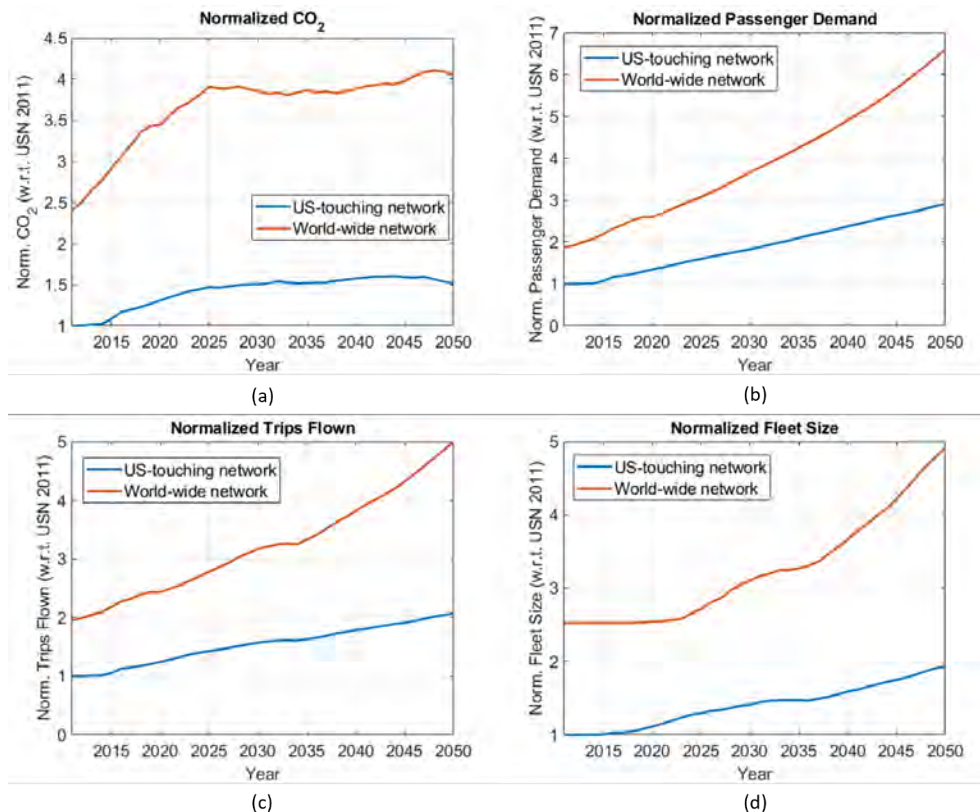


Figure 34. Normalized CO₂ emissions (a), normalized passenger demand (b), normalized trips flown (c), and normalized fleet size (d) for the worldwide network and US-touching network.

Similarly, Figure 34b compares the passenger demand in FLEET considering a worldwide network (depicted by the solid red line) with the passenger demand considering a US-touching only network (depicted by the solid blue line). The passenger demand for the worldwide network grows considerably faster than that of the US-touching network, which is consistent with what the team observed from the passenger demand data. Figure 34c and Figure 34d, respectively, show the increase in the number of trips flown and the fleet size when FLEET models a worldwide route network.

FLEET Allocation Results for Worldwide Operations (Simultaneous Subsonic and Supersonic)

In order to analyze worldwide airline operations that include the entry in service of a supersonic aircraft, the research team modified and update FLEET to (1) ingest the worldwide demand and fleet characteristics, and (2) solve the resource allocation problem while considering the introduction of the supersonic aircraft. Assuming an entry-in-service date of 2024 for the SST concept and using the demand evolution assumptions described in previous reports leads to the projected travel demand and associated emissions shown in Figure 35. These are initial estimates of the impact of introducing a 55-passenger, Mach 2.2 cruise number SST; at the time of this report, additional work is underway to assess the quality of these results.

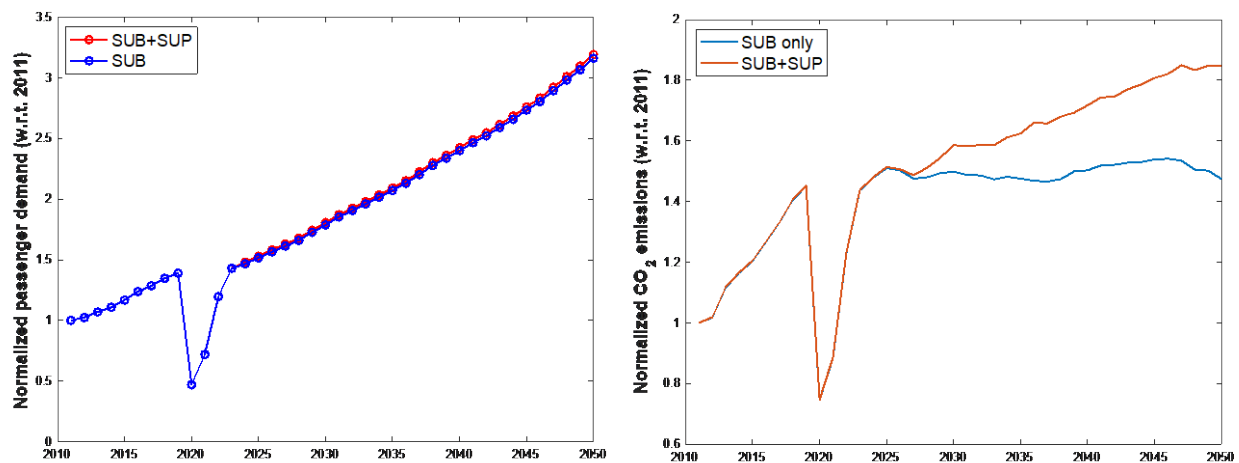


Figure 35. Initial estimates of travel demand and associated emissions, normalized to 2011 levels.

Travel demand reflects historical data until 2019, a steep drop associated with early estimates of air travel demand decrease associated with the COVID-19 pandemic, and then makes assumptions about a potential recovery scenario following COVID-19. As discussed earlier, we assume that up to 5% of travel demand can be served by the SST. As Figure 35 (right) shows, the emissions contributions of SSTs are considerable. In fact, a ~37% increase in 2050 emissions levels is due to the SST. The combination of high fuel burn and low passenger capacity of this aircraft concept results in this estimation. This contribution to emissions is even more clear when observing the emission levels that each aircraft class and technology group contribute. Figure 36 (left) presents the normalized emissions that each aircraft class contributes to total emission levels and Figure 36 (right) presents the contribution grouped by technology (RIC: representative-in-class aircraft; BIC: best-in-class aircraft; NIC: new-in-class aircraft; FIC: future-in-class aircraft; SST: supersonic transport).

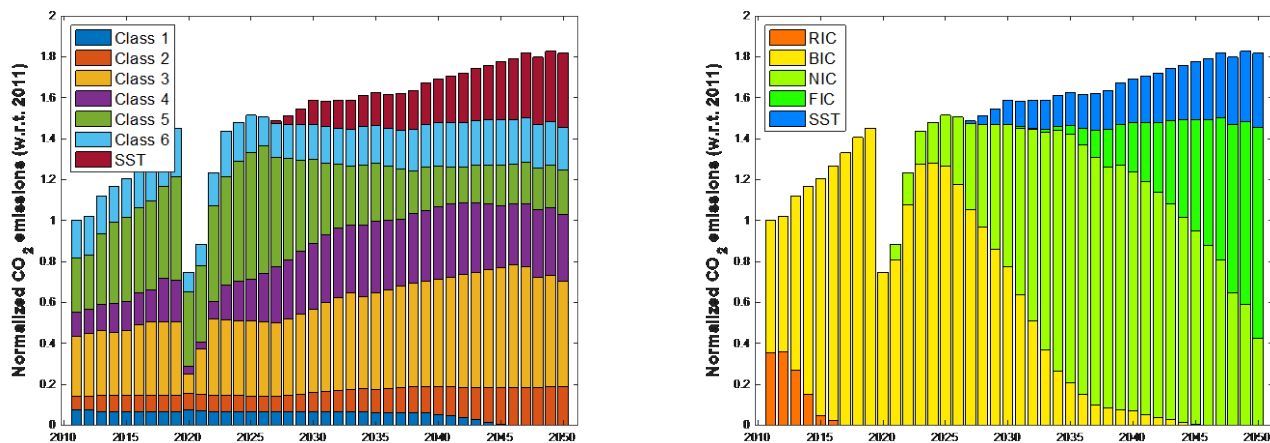


Figure 36. Emissions contribution of aircraft fleets and technology groups. RIC, representative-in-class aircraft; BIC, best-in-class aircraft; NIC, new-in-class aircraft; FIC, future-in-class aircraft; SST, supersonic transport.

Even as demand continues to grow (passenger trip demand is roughly 3.2 times larger in 2050 than in 2011), the introduction of more fuel-efficient subsonic aircraft manages to maintain 2025 emission levels. However, the introduction and use of the SST results in an overall increase in emission levels with respect to the 2011 baseline in these initial results. Future work will investigate the impact that alternate demand evolution scenarios, SST fuel-burn assumptions, and even alternate SST concepts have on the expected emissions and environmental impact of aviation.

Subtask 3: Analysis of Alternate SST Concepts

Simple SST Sizing Approach (Placeholder 2.0)

In previous work, the authors utilized a 55-seat “placeholder” commercial supersonic aircraft model to identify potential supersonic routes in a US-touching route network; the placeholder model was based on Boom’s Overture concept with an over-water supersonic cruise speed of Mach 2.2 and an over-land subsonic cruise speed of Mach 0.95. The authors use the “placeholder” notation because these aircraft models were used only for identifying potential supersonic routes and have been replaced in FLEET simulations by higher-fidelity supersonic aircraft models. These higher-fidelity models were developed by colleagues at Georgia Tech. The maximum range of the placeholder aircraft was designated to be 4,500 nmi. The L/D ratio and the specific fuel consumption (SFC) value for sizing the placeholder supersonic aircraft were based on some improvements over Concorde’s values. For performance calculations, the over-land segment was assumed to be equally split at each end of the over-water segment. In reality, the over-land segment is airport pair- and route-dependent (e.g., for one airport pair, the origin might be close to the ocean and the destination further inland; the return flight on this pair would have the opposite), so a higher-resolution representation of the routes for aircraft performance calculations will lead to different fuel burn characteristics for each direction on each route.

For this work, the authors develop an updated version of the placeholder commercial supersonic aircraft model, dubbed the “placeholder v2.0” aircraft model. The L/D ratio and SFC value for the placeholder v2.0 model are based on the higher-fidelity supersonic aircraft models developed by our colleagues at Georgia Tech. Additionally, the placeholder v2.0 model takes into account the higher-resolution representation of the routes for aircraft performance calculations, allowing it to reflect the difference in fuel burn (and the aircraft range capability) for each direction on each route.

This work includes different size and speed supersonic aircraft in the FLEET simulations. The set includes 55-seat, 75-seat, and 100-seat supersonic aircraft operating at multiple supersonic cruise speeds.

Table 20. Alternate supersonic transport concepts (developed by Georgia Tech).

Vehicle Seating Capacity	Supersonic Cruise Mach Number		
55 passengers	1.8	2.0	2.2
75 passengers	2.2	2.2	2.2
100 passengers	1.6	1.8	2.0

Each combination of seat capacity and cruise speed leads to a different aircraft configuration, with the higher-fidelity models provided by our colleagues at Georgia Tech. This leads to a total of seven aircraft available for implementation in FLEET. The authors adapt the placeholder v2.0 aircraft model to depict all seven aircraft and identify potential supersonic routes for each aircraft type.

Supersonic Flight Path Calculations

Previous work relied on a simplistic method of flight path calculation, whereas the distance flown is calculated from the great circle path distance. The over-land and over-water distances were calculated by dividing the total distance by given fixed over-water percentages. The work presented in this paper uses a polygon approach to calculate accurate over-water distances, whereas the intersection between the flight path and the coastline separates over-land and over-water segments. The block time is then simply calculated by dividing segment distance by over-land or over-water airspeed. This approach also takes into account the differences in fuel burn when flying in different directions on the same route, i.e., when flying from A to B and B to A.

The block time for each origin destination pair is calculated as follows:

1. Calculate the great circle path between the origin airport and the destination airport of a route.
2. Deviate the midpoint by $\pm 7^\circ$ with 1° intervals along the direction perpendicular to the heading at midpoint.
3. Separated each route by land-water intersections into k segments.
4. Calculate the distances of each segment and record the sum of over-water distances.
5. Calculate block time of each route option.
6. Find the minimum block time path for both forward and return directions.

The block time calculation follows the equation below, where k is the total number of segments within the route, d_k is the distance of segment k , and V_k is the airspeed at that segment. Because all supersonic operations are restricted to over-water, aircraft fly at $V_{supersonic}$ on over-water segments and at $V_{subsonic}$ on over-land segments.

$$block\ time = \sum_{k=1}^N \frac{d_k}{V_k}$$

$$V_k = V_{supersonic} \ (k \subset over-water\ segment)$$

$$V_k = V_{subsonic} \ (k \subset over-land\ segment)$$

All available nonstop routes are found by filtering all routes by range. To extend flight range, a search algorithm finds all available fuel stops along the path for each OD pair. The routes with fuel stops are again filtered based on the design range of “placeholder v2.0” aircraft.

Identification of SST-Eligible Routes – Nonstop Routes

Nonstop supersonic routes—like the example route, LAX–TPE, shown in Figure 37—are shorter than 4,500 nmi and do not require a fuel stop (shown in the figure, midpoints are deviated by $\pm 7^\circ$ with 1° increments). The green lines represent the deviated routes and the red triangles represent midpoints of each route. As shown in the figure, the top route path has more overlap with land, which would increase block time. In this case, the bottom route path has the least block time, and it is the best route for the example in consideration.

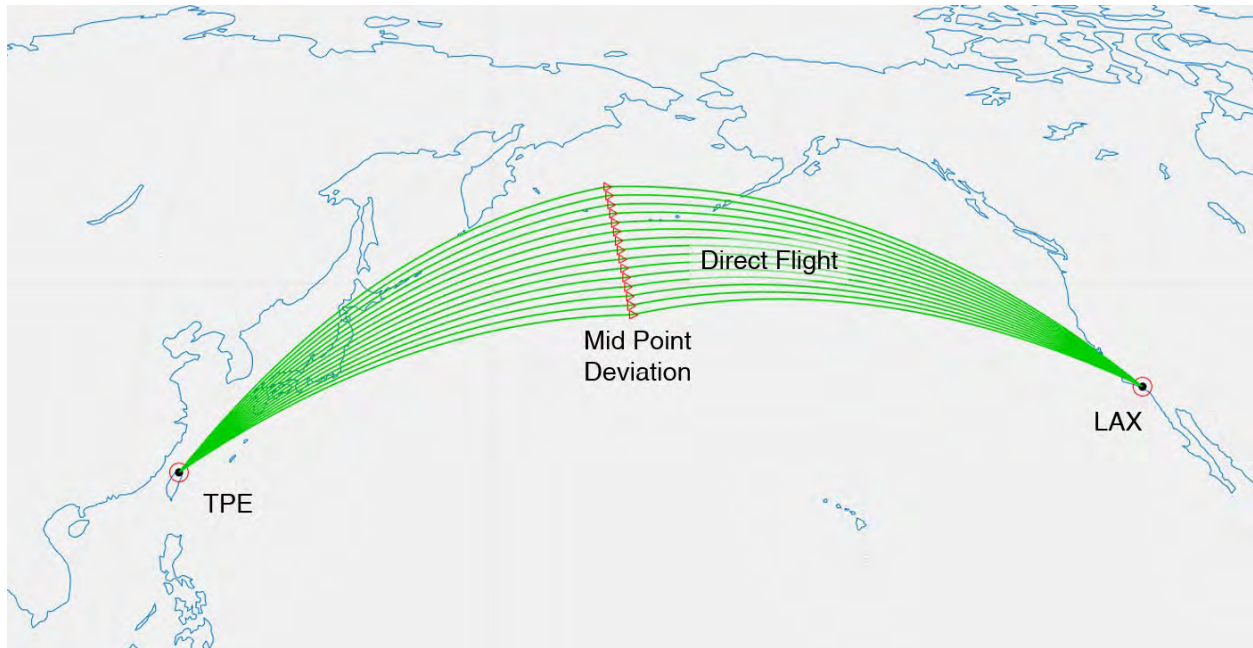


Figure 37. Example supersonic route (LAX-TPE) that does not require a fuel stop.

Identification of SST-Eligible Routes – Routes With Fuel Stops

Earlier, the fuel stop options for routes longer than 4,500 nmi only included Honolulu, Hawaii (HNL) and Anchorage, Alaska (ANC) for cross-Pacific routes, and Shannon, Ireland (SNN); Keflavik, Iceland (KEF); Oslo, Norway (OSL); and San Juan, Puerto Rico (SJU) for cross-Atlantic routes. This approach was valid only for the US-touching route network and required manual inputs to select the appropriate fuel stop. To capture fuel stops for all global routes, an automated area-search method is developed and implemented. For each OD pair, a search area is placed on the great circle path between them. All airports within the area would be captured as potential fuel stops. To avoid the case where the supersonic aircraft lands for a fuel stop immediately after takeoff, a circular search area is placed at the route's midpoint to ensure airports in the vicinity of the origin or the destination are not captured. The diameter of the search area is set to 35° spherical arc to include maximum possible fuel stop options; the arc size was based on trial and error.

With each fuel stop, a deviation process similar to nonstop supersonic routes is implemented for both segments and both directions to find the minimum block time path of each path. In the case shown in Figure 38, HNL and ANC are selected as fuel stop options for the LAX-TPE route. The gray routes shown in the figure depict the deviated routes with fuel stops, whereas the red triangles depict the midpoints for each deviated route; the red route path represents the path with minimum block time.

The fuel required to fly any such route is calculated by modeling both segments of the route, accounting for the departure and arrival of each segment, and the block time accounts for the extra time required to land and take off at the fuel stop airport.

Higher-Resolution Supersonic Aircraft Modeling and Routing

The computational models of the 55-seat, 75-seat, and 100-seat supersonic aircraft for this study are developed by colleagues at Georgia Tech. These models provide mission performance characteristics, including fuel consumption and block time, for the supersonic aircraft to operate on routes in the FLEET network. Because the supersonic aircraft can only operate at supersonic speed over water, the ground path of the flight to optimize a combination of fuel consumption and block time can deviate significantly from typical subsonic aircraft routes. For consistency in the ASCENT project, the studies presented here also use flight path ground tracks generated by teammates at Georgia Tech.

The Purdue team considers two generations of supersonic aircraft with entry-into-service (EIS) dates of 2025 (generation 1) and 2038 (generation 2). The generation 2 supersonic aircraft show a 10% improvement in fuel burn with no change in aircraft noise or sonic boom characteristics.

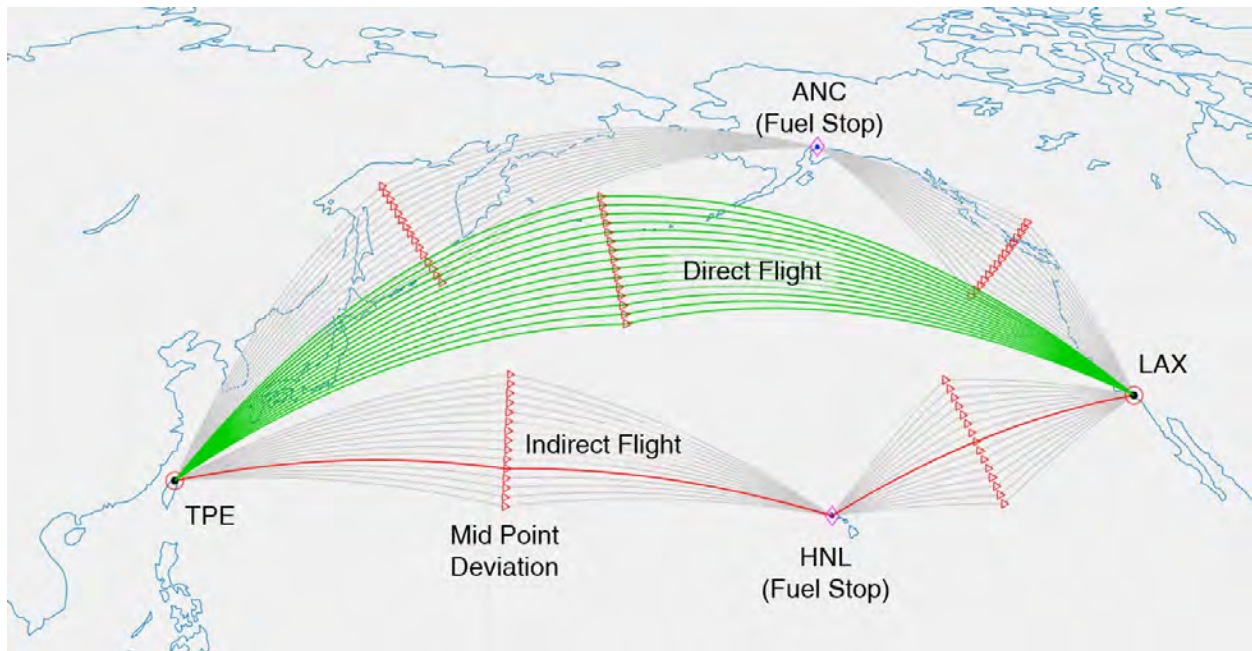


Figure 38. Example supersonic route that requires a fuel stop.

The detailed supersonic routing developed by Georgia Tech works to identify the optimum supersonic route path by solving an optimization problem to minimize a weighted sum “cost to the goal” objective function. The goal here is to minimize a combination of block time and block fuel values for flying supersonic aircraft on a supersonic route. This approach essentially finds a supersonic route path that is a tradeoff between the time optimal-only route and fuel optimal-only supersonic route path. A simplistic representation of this approach is:

$$weightedsum_{objective} = \alpha * \frac{BlockFuel}{BlockFuel_{min}} + (1 - \alpha) * \frac{BlockTime}{BlockTime_{min}}$$

Current work uses $\alpha = 0.4$ as the recommended value for the weighted sum supersonic routing (based on various supersonic routing tests conducted by our partners at Georgia Tech). The authors use FLOPSv9 to “fly” the detailed supersonic aircraft models on the weighted sum routes, conducting separate FLOPS runs for each direction of a supersonic route; the team observed different block fuel values (and in some cases, block time) when flying the detailed notional supersonic aircraft in different directions on a supersonic route.

Subtask 4: FLEET for Business Jet Operations

To increase the value and utility of FLEET in assessing the environmental impact of aviation beyond airline operations, the Purdue Team began work to expand FLEET to model and analyze business jet operations. The goal of this effort is to create a baseline modeling capability that can be expanded and improved in its fidelity in possible follow-on work. Developing FLEET-B entails four efforts:

- Modeling of business jet travel demand
- Representation and modeling of business jet fleet of aircraft
- Modeling of business jet resource allocation
- Evolution of business jet operations (fleet of aircraft and demand)

Business Jet Travel Demand

Data provided by the Common Operations Database (COD) for 2018 [35] represents worldwide travel on business jets for 2018. The data contain the operations of 11,214 companies; however, only a small fraction of these companies provide the most and somewhat regular service. For the purpose of this work, we define regular service by a company if four or more daily trips are flown. With this assumption, only 2% of the companies (217) flew more than four daily trips and provided 50% of business jet travel in 2018.

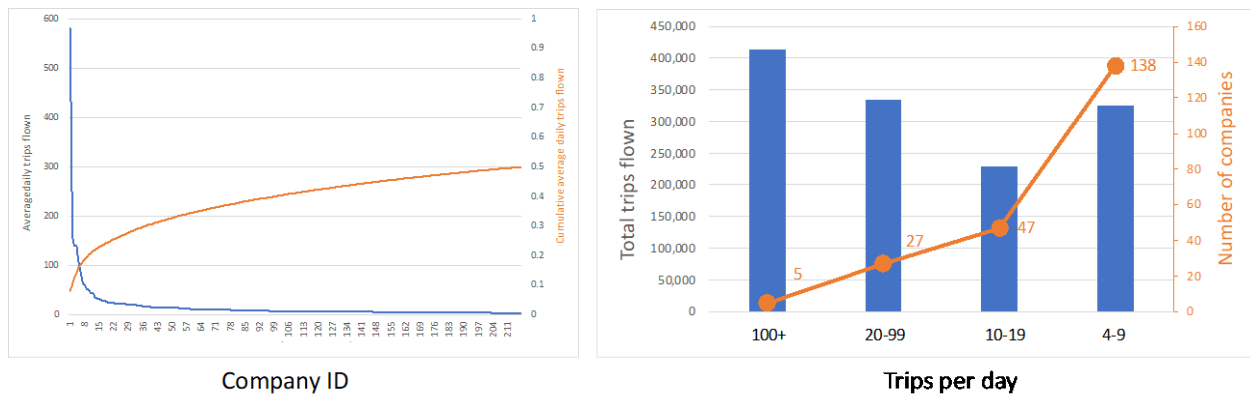


Figure 39. Companies providing business jet services in 2018.

Furthermore, less than half of these 217 companies had a high level of operation, reaching more than 10 daily trips (Figure 39, right). Fractional operators Netjets, Privair, and Bombardier Jet Solutions were the companies providing most of the activity in 2018. The other companies were a mix of fractional, charter, air taxi, and corporate operators. The activity of these operators consisted of ~1.3 million trips between ~160,000 city-pairs among 4,417 airports.

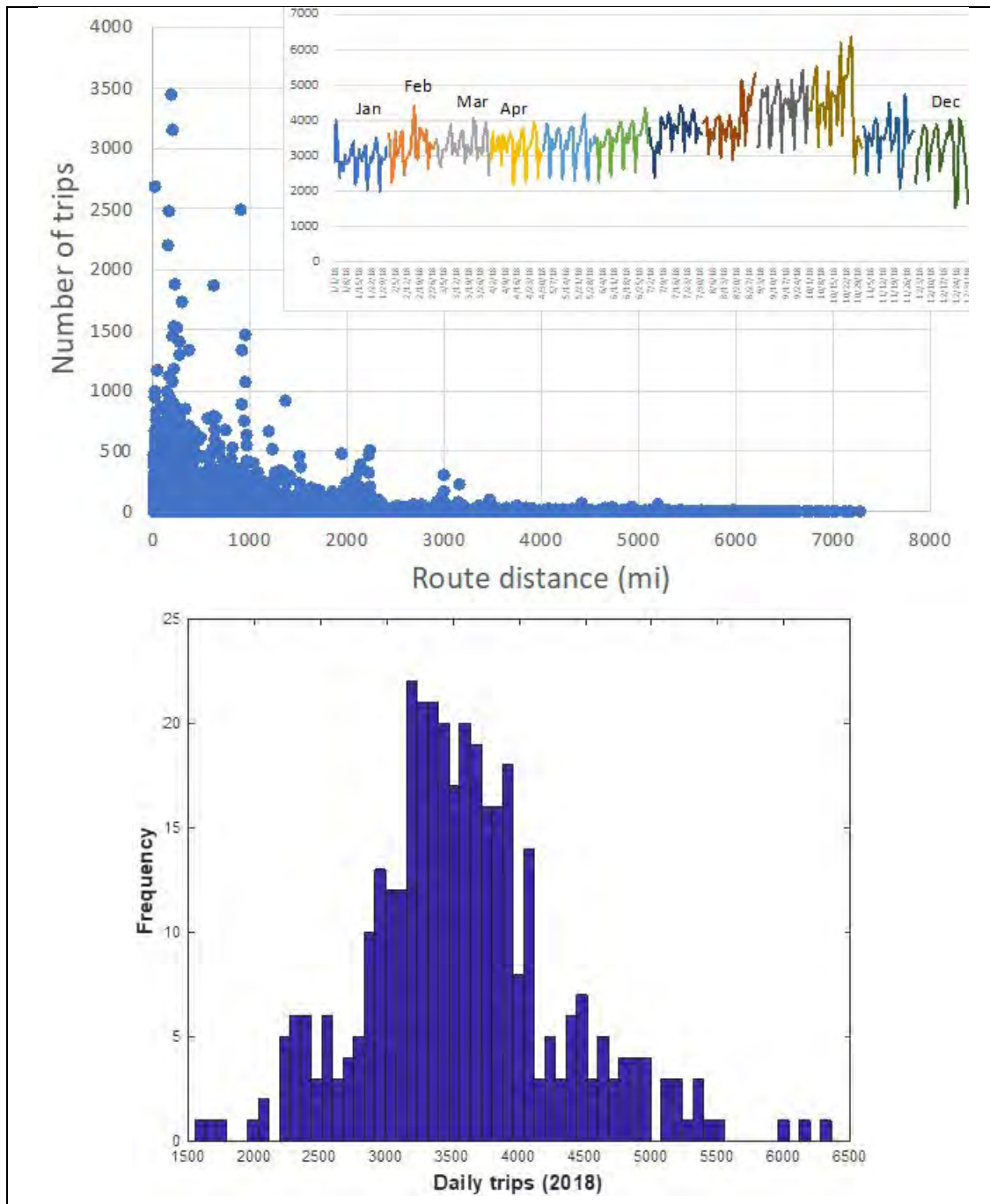


Figure 40. Trip distribution of business jet travel; top: number of trips and route distance; bottom: daily trip distribution.

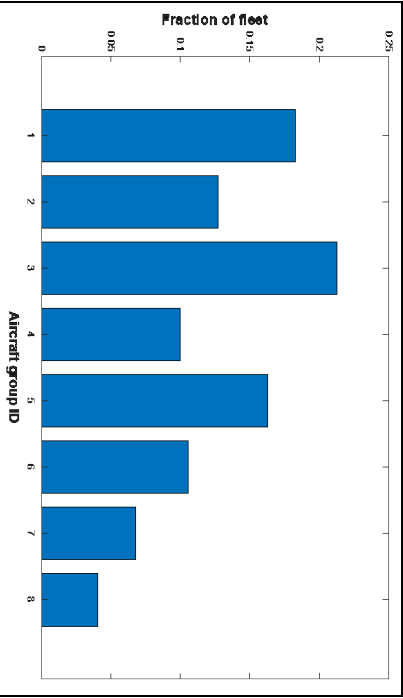
Directly applying the current resource allocation model in FLEET to represent and analyze the level of operations presented here is infeasible. Because the combined number of airports, city-pairs, and trips is too large for the model to generate a solution in any reasonable time, we group the daily trips into 50-mile bins. This generates a total of 146 route-bins for the

city-pair distances between 0 and 7,300 miles. This assumption greatly reduces and simplifies the allocation model, but it retains the ability to estimate the number of aircraft required to meet all trip demand and their emissions. However, this approach eliminates the ability to capture the number of operations at any given airport, because any given route-distance bin contains many different city-pairs and airports.

Aircraft Fleet Size and Mix

The data provided by COD also contains information about the type of aircraft used to provide the service for each company. The aircraft are also grouped into categories based on their size and range. Table 21 presents these groups of aircraft, exemplars for each, and the fraction of aircraft in the fleet.

Table 21. Aircraft flown by business jet operators.

Aircraft type ID	Aircraft Category	Exemplars	<div>  </div>
B1	BJ 1.5 Very Light Jet	Embraer 500, Citation M2, etc.	
B2	BJ 2.0 Light Jet	Beechjet 400, Citation V, Premier I, etc.	
B3	BJ 3.0 Light Jet	Citation XLS, Lear 60, Lear 45	
B4	BJ 3.5 Light Jet	Citation Sovereign, Falcon 50, Hawker 800	
B5	BJ 4.0 Medium	Challenger 300, Hawker 1000, Citation X	
B6	BJ 5.0 Medium	Falcon 2000, Challenger 604	
B7	BJ 6.0 Large	G450, G5000, Falcon 900EX	
B8	BJ 7.0 Large	Falcon 7X, Global 6000, Falcon 8X	
	BJ 7.5 Large	G650	
	BJ 8.0 Corporate	B737-700, A319-100	
	BJ 8.5 Corporate Very Large	B777-200, B787-8	

Because the number and operations of category 7.5, 8.0, and 8.5 were very small, they are included in aircraft type ID B8 in this study. Most of the service is provided by group B1, followed by group B3, and then B2. Figure 41 shows the daily trip distribution for each of these groups of aircraft. This will be the basis for the trip demand on which the aircraft allocation problem will be solved.

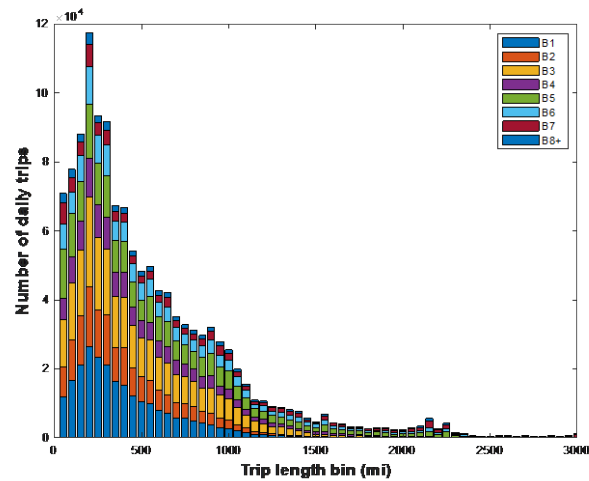


Figure 41. Daily trip distribution by aircraft group.

To allocate aircraft properly to satisfy demand, the FLEET tool requires information about each aircraft's performance and cost. For the analysis of airline operations, the team has developed FLOPS models that provide performance and cost estimations. Similar models are needed to fully develop FLEET into FLEET-B. However, for the purposes of this current effort (to demonstrate the utility of a business jet version of FLEET), we estimate the cost to operate each group of aircraft by using historical data. Figure 42 presents the available cost information as a function of aircraft range and the DOC of each group of aircraft based on the exemplar aircraft in each group. The three sets of data fits shown here are based on different aircraft speeds, and the fit selected to estimate the aircraft cost is the one that most closely approximates the performance of the exemplar aircraft.

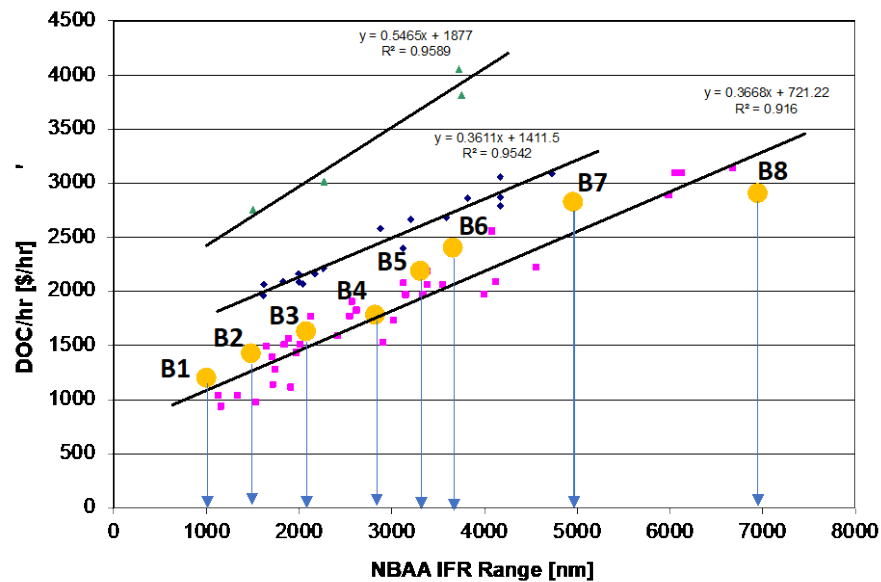


Figure 42. Direct operating cost (DOC) of aircraft considered in study. NBAA IFR, National Business Aviation Association instrument flight rules.



With this information at hand, the input parameters for the resource allocation model are complete. We note that the goal of this effort is to demonstrate the utility of the analysis and create a foundation upon which to refine the model with more accurate aircraft performance parameters, demand information, and fleet and demand evolution in the future.

Resource Allocation Model

Business jet operations, and the companies that provide this type of service, are different from airline operations. While both provide a transportation service, business jet operations are governed less by a need to fulfill passenger-based travel and more by trip-based travel. In other words, the primary goal of business jet operations is to satisfy trip demand and not necessarily passenger demand. For corporate operators, for example, the decision to acquire an aircraft with a given passenger capacity dictates the number of passengers that can be carried on a given trip, and the only decision during operations is whether to use the aircraft or not. Similarly, fractional share owners decide the type of aircraft in which they want to own a share based on its performance characteristics, then only decide when and where to fly within those constraints. The daily decisions of a fractional operator center on how to allocate aircraft to meet the trip demand of specific owners in the least costly manner, not how to fill seats on the aircraft.

If a supersonic business jet (SSBJ) is considered as an addition to the fleet of aircraft, the decision on how to use that aircraft would be similar. Because the primary benefit of an SSBJ is the reduction in travel time, the allocation model would need to accommodate and account for this. Based on this type of operation and decision-making, we define the following decision variables and parameters:

Sets:

c = company type (fractional, charter, air taxi, corporate)

k = aircraft type

j = route

Variables:

$trips_{c,k,j}$ = number of trips flown by company c on aircraft k and route j

$trips_{c,s,j}$ = number of trips flown by company c on SST aircraft s and route j

$aircraft_hours_{c,k}$ = number of aircraft-hours flown by company c on aircraft k

$fleet_used_{c,k}$ = number of aircraft used by company c of type k

Parameters:

$C_{c,k,j}$ = cost for company c to fly aircraft type k on route j

$dem_{c,k,j}$ = number of trips of company c aircraft type k on route j

$fleet_{c,k}$ = fleet size (number of aircraft) for company c of type k

$AA_{c,k}$ = aircraft availability for company c of type k

$OH_{c,k}$ = operational hours for company c of type k

$BH_{c,k,j}$ = block time of company c for aircraft type k on route j

$MH_{c,k,j}$ = maintenance of company c hour for aircraft type k on route j

$DH_{c,k,j}$ = deadhead hours of company c hour for aircraft type k on route j

t_c = aircraft turnaround time for company c

$(tt_{sub})_{c,j}$ = average travel time of subsonic aircraft operated by company c on route j

$(tt_{sup})_{c,j}$ = travel time of supersonic aircraft operated by company c on route j

$(value\ of\ time)_c$ = value of travel time for customers of company c

We formulate the resource allocation of business jet operations as follows:

$$\text{Min} \left(\sum_{c=1}^C \sum_{k=1}^K \sum_{j=1}^J trips_{c,k,j} C_{c,k,j} - \sum_{c=1}^C \sum_{j=1}^J savings_{c,j} \right) + M \sum_{c=1}^C \sum_{k=1}^K fleet_{used_{c,k}} \quad (1)$$

where

$$savings_{c,j} = [(tt_{sub})_{c,j} - (tt_{sup})_{c,j}] \times (value\ of\ time)_c \quad (2)$$

Subject to



$$trips_{c,k',j} + trips_{c,s,j} \geq dem_{c,k,j} \quad \forall (k' + s) \in k \quad (3)$$

$$\sum_{j=1}^J trip_{c,k,j} (BH_{c,k,j} + DH_{c,k,j} + MH_{c,k,j} + t_c) = aircraft_hours_{c,k} \quad (4)$$

$$aircraft_hours_{c,k} \leq fleet_used_{c,k} \cdot AA_{c,k} \cdot OH_{c,k} \quad (5)$$

$$fleet_used_{c,k} \leq fleet_{c,k} \quad (6)$$

The objective function (Eq 1) aims to minimize the cost of satisfying the trip demand while also minimizing the number of aircraft used, captured here by the big-M quantity. The cost to fly the demanded trips accounts for the value of travel time and the expected travel time savings when the value of travel time is taken into consideration (represented by Eq 2). The constraints represented by Equation 3 ensure that the number of trips flown on subsonic and supersonic aircraft satisfy all demanded trips on each aircraft type, for each company, and on each route. Equation 4 calculates the number of aircraft-hours required to fly all trips for each aircraft type and company when taking into consideration block hours flown and deadhead time (repositioning flights that do not carry passengers, maintenance time, and turnaround time). Constraints in Eq 5 ensure that we capture the aircraft availability ($AA_{c,k}$) and the number of operational hours that the company has available to satisfy daily demand ($OH_{c,k}$). This last parameter is designed to capture the different types of operations and scheduling requirements of different companies and business models. For example, the daily travel demand of a corporate operator is very different from that of a fractional operator. A corporate operator may only have two trips in a given day, but those trips happen at the same time, which means that they may require two aircraft to satisfy demand. A fractional operator, on the other hand, may have 10 trips in a day, but if they occur in two-hour intervals and are less than 1-hour trips, then the company may only need 2 to 5 aircraft to satisfy that demand. For the purposes of this demonstration model, we make assumptions about these parameters and will research possible data sources to obtain more realistic values and values that accurately estimate and capture the operational tempo of different operators. Finally, the constraints in Equation 6 ensure that the number of aircraft required to satisfy all demand (when accounting for the operational realities of the company) does not exceed the available fleet size.

Results

Solving the above allocation problem for daily demand and the aircraft models described earlier is relatively fast. Because the number of routes is only 146, GAMS and its algorithms are able to generate a solution in a few seconds. We solve the allocation model for each day of operations and are able to generate statistics of the results. Figure 43 presents these results when only subsonic aircraft are considered and when we assume that there is only one company satisfying all travel demand.

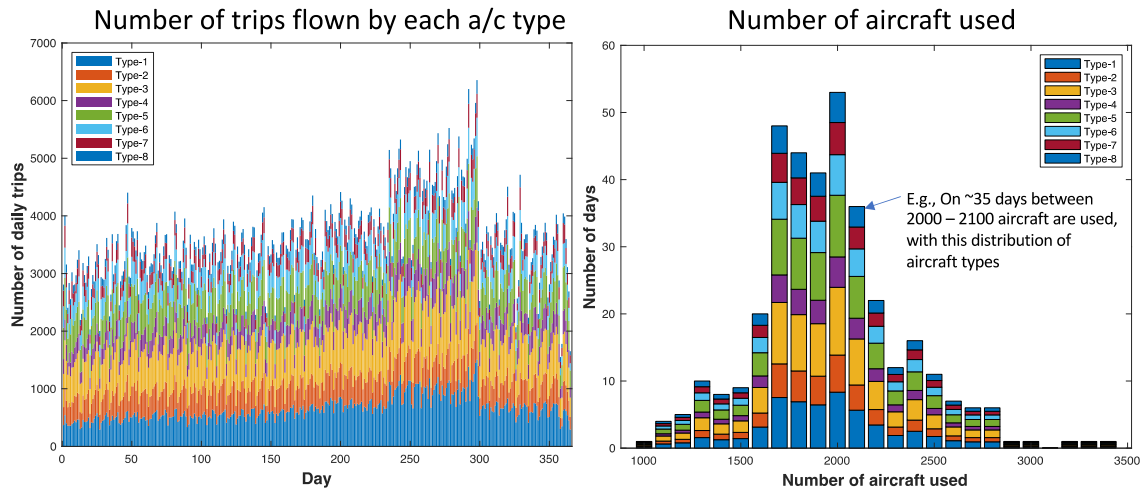


Figure 43. Aircraft allocation results assuming single-operator and subsonic-only aircraft to demonstrate potential capability of the FLEET-B simulation.

Recall that demand is specified for each route and for each aircraft type; therefore, the decision made by the resource allocation model is to identify the number of aircraft required to satisfy demand. The ability to analyze each day of operation makes possible the identification of the distribution of the number of aircraft that are needed to satisfy demand. Figure 43 (right) clearly displays these results by providing the number of days that a given number of aircraft is required. For example, on 35 days of the year, between 2,000 and 2,100 aircraft are used to satisfy all demand. An interesting implication of this type of result is that it is clear how the fleet size for a given operator may be driven not by the average number of operations but by the busiest day. The simplicity of the allocation model (only 146 binned routes) facilitates this analysis and observation.

When introducing the supersonic aircraft to the available fleet of aircraft, it is necessary to include its speed and cost in the allocation model. Figure 44 (left) provides an overview of the difference in travel time that an SSBJ can offer compared to subsonic aircraft, and Figure 44 (right) provides a similar comparison for the cost. We assume here that for trip distances less than 600 mi, a supersonic aircraft would not be able to get up to supersonic speeds, hence the similar block time for those distances.

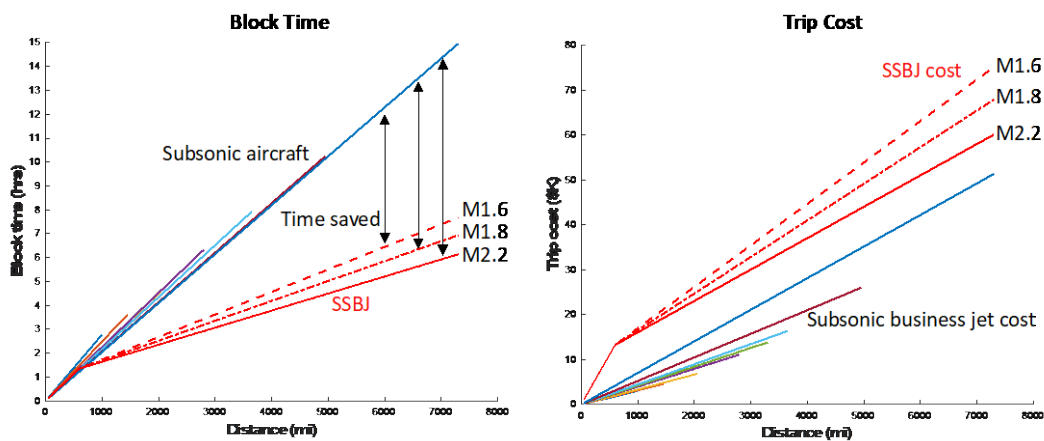


Figure 44. Block time and trip cost of subsonic and supersonic business jets (SSBJ).

Because the advantage of SSBJ is in the travel time savings, and as shown in the description of the resource allocation model, we include this travel benefit in the model by defining an effective trip cost that reduces the cost to operate the aircraft by the value of travel time savings (Eq 2). Figure 45 presents the effect of this adjustment on the trip cost when different values of travel time are considered.

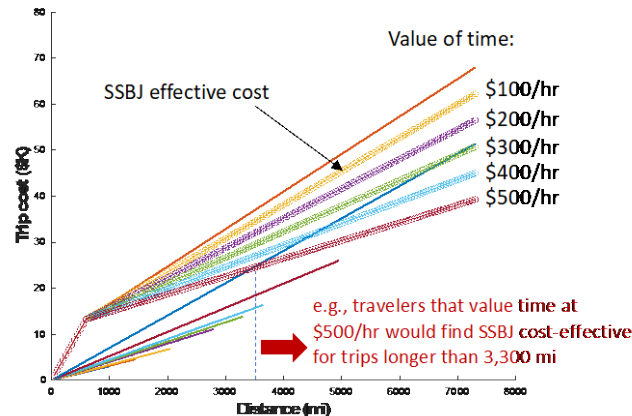


Figure 45. Trip cost when accounting for value of travel time savings. SSBJ, supersonic business jet.

For example, for those travelers who value time at \$500/hr or more, trips longer than 3,300 mi would be considered cost effective, and the effective trip cost would be less than the trip cost if flown on a subsonic aircraft. By using these data and by making the supersonic aircraft an option for any trip and a substitute for any aircraft type, the allocation model is able to determine on which routes the use of an SSBJ would be cost effective when all components of travel time (block time, turnaround time) and operational requirements (maintenance time, repositioning time) are considered. We highlight that no assumptions are made a priori about the routes on which an SSBJ would be available. It is the allocation model that determines the routes on which an SSBJ is cost effective.

Therefore, when accounting for the value of travel time savings and including the SSBJ aircraft in the allocation model, it is possible to identify which routes could see supersonic service. Figure 46 (left) presents the number of trips that are flown on each route-bin by an SSBJ that is able to cruise at M1.6 for values of time of \$500/hr, \$400/hr, and \$300/hr; Figure 46 (right) shows the total number of trips that would be flown for SSBJ of M1.6, M1.8, and M2.2 as a function of the value of travel time.

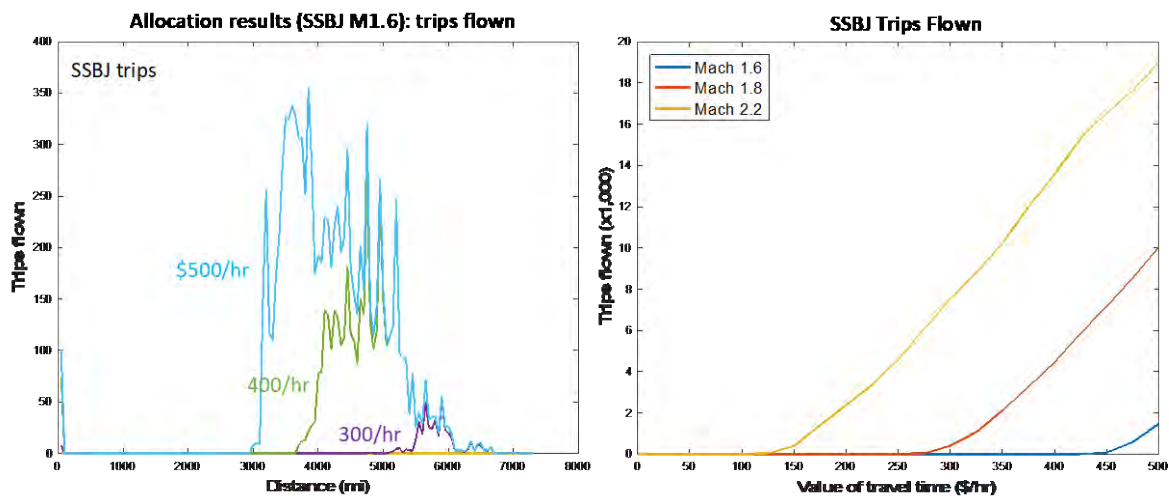


Figure 46. Level of service provided for varying values of travel time. SSBJ, supersonic business jet.

As expected, when the value of time is large, SSBJ travel time savings are sufficient to offset the trip cost. As the value of travel time increases, the number of trips flown also increases. Furthermore, the faster the SSBJ, the greater the travel time savings, and therefore the larger the number of trips flown on the SSBJ. Although several simplifying assumptions are made here to demonstrate the viability of this type of analysis, the model shows that it is possible to capture the possible decision-making of business jet operators and to account for the benefits of supersonic travel.

Future Work

Further work on this task will entail improving the fidelity of the subsonic and supersonic aircraft models to generate better approximation of ownership and operating costs. Refinement of the operational model of the various types of business jet operators is another area of improvement that will increase the fidelity of the analysis. Identifying meaningful assumptions about the daily operating hours of each operator will enable the model to more accurately estimate the number of aircraft required to satisfy demand. While the estimation of fuel burn, environmental emissions, and number of operations at a given airport would not be affected by this, the ability to estimate the degree of penetration of supersonic aircraft in the fleet mix and the evolution of new aircraft and associated aircraft technologies will require more accurate information.

Outreach Efforts

During this period of performance, the Georgia Tech team published the following:

Baltman, E., Tai, J. C., Ahuja, J., Stewart, B., Perron, C., De Azevedo, J., Vlady, T. R., & Mavris, D. N. (2022). A Methodology for Determining the Interdependence of Fuel Burn and LTO Noise of a Commercial Supersonic Transport. AIAA AVIATION 2022 Forum, 1–16. <https://doi.org/10.2514/6.2022-4110>

During this period of research, the Purdue team published the following:

Yang, B., Mane, M., and Crossley, W. (2022). An Approach to Evaluate Fleet Level CO₂ Impact of Introducing Liquid-Hydrogen Aircraft to a World-Wide Network, AIAA Aviation Forum 2022, <https://doi.org/10.2514/6.2022-3313>

Jain, S., H. Chao, M. Mane, W. A. Crossley and D. A. DeLaurentis. (2021). Estimating the Reduction in Future Fleet-Level CO₂ Emissions From Sustainable Aviation Fuel, Frontiers in Energy Research, Nov 2021, doi: 10.3389/fenrg.2021.771705

Awards

None.

Student Involvement

The Purdue team included four graduate students during this year's effort, all of whom have been conducting tasks in support of the project. Samarth Jain finished his PhD studies, Suzanne Swaine continued her MS work, Fung Tien-Yueh continued his PhD work, Boning Yang finished his MS work and graduated.

The GT team also included the following graduate students during this year's effort: Nikhil Iyengar, Barbara Sampaio, Edan Baltman, Joao De Azevedo, Jiajie (Terry) Wen, Ted Vlady, Zayne Roohi and Srikanth Tindivanam Varadharajan

The GT team also trained one undergraduate student, Madeleine Graham, in matters related to CFD and optimization using the 65 pax Mach 1.7 baseline configuration as a starting point

Plans for Next Period

Georgia Tech

The plan for the next period of performance is to apply the improved design methodology presented in the current report to a wider set of supersonic vehicles. Specifically, the same process previously used for a 65-passenger SST vehicle with a cruise speed of Mach 1.7, will be applied to a similarly sized vehicle, but with a cruise speed of Mach 2.0. The Georgia Tech team will also examine an SST vehicle designed for a lower cruise speed of Mach 1.4, still with a 65-passenger capacity. Finally, a supersonic business jet with an 8-passenger capacity and a cruise speed of Mach 1.4 will be investigated. This last vehicle will notably be designed with only two engines due to its smaller scale, unlike the 4 engines configuration used for the other SST aircraft. The fuel burn and the LTO noise for each of the proposed configurations will be captured and

compared, allowing us to investigate the interdependence of both metrics with more granularity. The analysis of these SST vehicles will also be performed with an updated demand forecast.

References

- [1] Haimes, R., & Dannenheffer, J. F. (2013, June 24-27). *The engineering sketch pad: A solid-modeling, feature-based, web-enabled system for building parametric geometry* [Conference presentation]. 21st AIAA Computational Fluid Dynamics Conference, San Diego, CA. <https://doi.org/10.2514/6.2013-3073>
- [2] NASA Advanced Supercomputing Division, (n.d.) *Cart3D Documentation* <https://www.nas.nasa.gov/publications/software/docs/cart3d/>
- [3] Siemens. (n.d.) *Simcenter STAR-CCM+*. <https://www.plm.automation.siemens.com/global/en/products/simcenter/STAR-CCM.html>
- [4] Constantine, P. G., Dow, E., & Wang, Q. (2014). Active subspace methods in theory and practice: Applications to Kriging surfaces. *SIAM Journal on Scientific Computing*, 36(4), 1500–1524. <https://doi.org/10.1137/130916138>
- [5] Tripathy, R., Bilonis, I., & Gonzalez, M. (2016). Gaussian processes with built-in dimensionality reduction: Applications to high-dimensional uncertainty propagation. *Journal of Computational Physics*, (321), 191–223. <https://doi.org/10.1016/j.jcp.2016.05.039>
- [6] Seshadri, P., Yuchi, S., & Parks, G. T. (2019). Dimension reduction via Gaussian ridge functions. *SIAM-ASA Journal on Uncertainty Quantification*, (7)4, 1301–1322. <https://doi.org/10.1137/18M1168571>
- [7] Gautier, R., Pandita, P., Ghosh, S., & Mavris, D. (2021). A fully Bayesian gradient-free supervised dimension reduction method using Gaussian processes. *International Journal for Uncertainty Quantification*, 12(2), 1–32.
- [8] Mulfti, B., Chen, M., Perron, C., & Mavris, D. N. (2022). *A multi-fidelity approximation of the active subspace method for surrogate models with high-dimensional inputs* [Conference presentation]. AIAA Aviation Forum, Chicago, IL. <https://doi.org/10.2514/6.2022-3488>
- [9] Jones, D. R., Schonlau, M., & Welch, W. J. (1998). Efficient global optimization of expensive black-box functions. *Journal of Global Optimization*, 13(4), 455–492. <https://doi.org/10.1023/A:1008306431147>
- [10] Forrester, A. I. J., & Keane, A. J. (2009). Recent advances in surrogate-based optimization. *Progress in Aerospace Sciences*, 45(1–3), 50–79. <https://doi.org/10.1016/j.paerosci.2008.11.001>
- [11] Wells, D. P., Horvath, B. L., & McCullers, L. A. (2017). *The flight optimization system weights estimation method*. NASA/TM-2017-219627
- [12] Han, Z.-H., and Görtz, S. (2012). Hierarchical Kriging model for variable-fidelity surrogate modeling. *AIAA Journal*, 50, 1885–1896. <https://doi.org/10.2514/1.J051354>
- [13] Lee, K., Nam, T., Perullo, C., & Mavris, D. N. (2011). Reduced-order modeling of a high-fidelity propulsion system simulation. *AIAA Journal*, 49(8). <https://doi.org/10.2514/1.J050887>
- [14] Mavris, D., Crossley, W., Tai, J., & Delaurentis, D. (2019). *Project 010 aircraft technology modeling and assessment*. <https://s3.wp.wsu.edu/uploads/sites/2479/2020/05/ASCENT-Project-010-2019-Annual-Report.pdf>
- [15] Walsh, P., Gas turbine performance
- [16] Frost, T., (1966) *Practical bypass mixing systems for fan jet aero engines*. <https://www.cambridge.org/core/journals/aeronautical-quarterly/article/practical-bypass-mixing-systems-for-fan-jet-aero-engines/8C316D80FD32E17F8A9A656A1DC6EFEA>
- [17] Zola, C., (2000) *Advanced propulsion system studies in high speed research*. <https://ntrs.nasa.gov/citations/20000057336>
- [18] McCullers, A. (1984). *Recent experiences in multidisciplinary analysis and optimization, Part 1*, NASA-CP-2327-PT-1, 395–412.
- [19] Computing with HTCondor. (n.d.) <https://research.cs.wisc.edu/htcondor/>
- [20] SAS Institute Inc. JMP®, Version 16. https://www.jmp.com/en_us/events/mastering/topics/new-in-jmp16-and-jmp-pro16.html
- [21] Baltman, E. M., Tai, J. C., Ahuja, J., Stewart, B., Perron, C., Azevedo, J. H. De, Vlady, T., & Mavris, D. N. (2022). A methodology for determining the interdependence of fuel burn and LTO noise of a commercial supersonic transport. *AIAA Aviation Forum*. <https://doi.org/https://doi.org/10.2514/6.2022-4110>
- [22] Raymer, D. P. (2018). *Aircraft design: a conceptual approach, Sixth Edition*. American Institute of Aeronautics and Astronautics, Inc.



- [23] Liebeck, R. H., Andrastek, D. A., Chau, J., Girvin, R., Lyon, R., Rawdon, B. K., Scott, P. W., & Wright, R. A. (1995). Advanced subsonic airplane design and economic studies. *Tech. Rep.* 19950017884. <https://ntrs.nasa.gov/citations/19950017884>
- [24] Air Transportation Association of America, (1967). Standard method of estimating comparative direct operating costs of turbine powered transport airplanes. *Tech. Rep.* <https://docplayer.net/39861253-Standard-method-of-estimating-comparative-direct-operating-costs-of-turbine-powered-transportairplanes.html>
- [25] Johnson, V. S. (1989). *Life cycle cost in the conceptual design of subsonic commercial aircraft*. [Ph.D. dissertation]. University of Kansas.
- [26] U.S. Bureau of Labor Statistics. *Cpi inflation calculator*. https://www.bls.gov/data/inflation_calculator.htm
- [27] Boeing Commercial. *About Boeing commercial airplanes*. <https://www.boeing.com/company/about-bca/>
- [28] Jane's Information Group. *Jane's all the world's aircraft*. <https://www.janes.com/publications/>
- [29] AeroCorner. *Archives: Aircraft*. <https://aerocorner.com/aircraft>
- [30] U.S. Department of Transportation, Bureau of Transportation Statistics. (n.d.) *Air carrier financial reports (form 41 financial data)*. [Online database]. https://www.transtats.bts.gov/databases.asp?Z1qr_VQ=E&Z1qr_Qr5p=N8vn6v10&f7owrp6_VQF=D
- [31] Moolchandani, K. (2012). *Impact of environmental constraints and aircraft technology on airline fleet composition*. [Master's thesis]. Purdue University.
- [32] Boeing. *Boeing current market outlook 2012-2031*. http://libraryonline.erau.edu/online-full-text/books-online/Boeing_Current_Market_Outlook_2012.pdf
- [33] Wyman, O. *Oliver Wyman global fleet & MRO market forecast summary 2017-2027*. <https://www.oliverwyman.com/our-expertise/insights/2017/feb/2017-2027-fleet-mro-forecast.html>
- [34] Mavris, D., Delaurentis, D., Crossley, W., & Alonso, J. J. (2017). *Project 10 aircraft technology modeling and assessment: Phase I report*. <https://ascent.aero/project/aircraft-technology-modeling-and-assessment/>
https://s3.wp.wsu.edu/uploads/sites/192/2017/10/ASCENT_P10_2017_PhaseI_Final_Report.pdf
- [35] Federal Aviation Administration, EUROCONTROL, ICAO's Committee on Aviation Environmental Protection (CAEP), U.S. Department of Transportation's Volpe Center, Common Operations Database (COD). (2018).
- [36] Official Airline Guide. (n.d.) *Traffic Analyser*. <https://www.oag.com/traffic-analyzer>